

# **Design and Implementation of a Loitering Controller for a Quadcopter using a GNSS, Barometer, and Time of Flight Sensor**

*Software & Electronic Systems Engineering*

Final Year Project 2023-2024

**Peter Davidson**

April 24, 2024

## **Declaration of Integrity**

I affirm that I am familiar with and have adhered to the plagiarism policies of Queen's University for this report, which is solely my own creation. This work has not been presented for any other assessment, and there has been no unauthorized collaboration. I certify that this report includes a comprehensive bibliography formatted according to the prescribed standards, accurately cites all secondary sources, and has been carefully reviewed to ensure compliance with the aforementioned requirements.

## **Acknowledgements**

I would like to thank Dr Pantelis Sopasakis and Mr Jamie Rainey for their continuous support throughout this project.

I would like to especially thank Dr Pantelis Sopasakis, invaluable technical assistance when it came to designing control algorithms, without said support the project would not have been completed.

## Original specification

Over the last couple of years, the Autonomous Systems Lab has been working on the development of bzzz – a radio-controlled quad-rotor (see <https://github.com/QUB-ASL/bzzz> for details). The quadcopter can now be flown in manual mode using a radio controller where the operator controls the total thrust directly, and in altitude hold mode where the quadcopter maintains a reference altitude. The next step is to make the quadcopter maintain a given reference (x, y, z)-position and heading. This is known as loitering mode operation. In this project, you will design and implement a loitering mode control system for bzzz. The main methodological tools for this will be the linear-quadratic regulator (LQR) and the Kalman filter. The estimation of the position of the quadcopter can be done using a GPS module in combination with other sensors (IMU and altimeter etc.).

## Problem Statement

Throughout this project I will be designing a loitering controller for a quadcopter. The objective of this is to enhance the quadcopters' ability to maintain a fixed position in space with high accuracy and minimal drift, this is a challenge in both commercial and civilian quadcopter use.

Loitering technology in quadcopters offers a range of benefits and applications. Security and surveillance, where home/business owners can have real time surveillance, programming a quadcopter to parole specific areas. As well as aerial photography and video, for those interested in photography or vlogging, quadcopters with loitering capabilities will allow for stable and high-quality aerial shots allowing for anything from time laps videos to landscape shots.

During the development of this project, I will be researching and implementing various concepts, these will vary from what sensors to get, control and estimation theory (using LQR, Kalman filter), python software development, PCB design and so on. I will elaborate more on these concepts below.

## Abstract

This project aims to enhance quadcopter navigation and stability through advanced sensor integration and control systems to achieve loitering control. Key objectives include; the parsing of GNSS data streams for latitude, longitude and altitude values, the parsing of barometer pressure readings and converting them into altitude values, design and implementation of a Kalman filter utilising sensor fusion for the Time of Flight, GNSS and barometer altitudes, the design of a PD controller for altitude hold and a PID controller for position hold, design of various different PCB's, 3D printed model designs. Finally, the completion of various hardware tasks around the quadcopter including building and soldering various components.

## **Objectives**

1. To design, implement and test a Kalman filter to estimate the (x, y, z)- position and the heading of the quadcopter using information from the IMU, the altimeter, and a GPS module.
2. To design, implement and test a control system for loitering.
3. To perform certain hardware tasks (proper mounting and connection of the GPS module to the on-board Raspberry Pi)
4. To perform experiments and record flight data

## **Learning Outcomes**

Upon successful completion of this project, I should:

1. Have mastered the theory of LQR and Kalman filtering.
2. Understand how a GPS module works and be able to interface it.
3. Be able to design a PCB.
4. Have a solid understanding of the attitude and translational dynamics of a quadcopter.
5. Be able to perform simulations of dynamical systems in Python.
6. Be able to operate a quadcopter using an RC.
7. Be able to integrate different systems involving hardware and software components.
8. Be able to use git and GitHub (branches, pull requests, etc).

This project will involve (25%) control and estimation theory of the LQR and the Kalman filter, (40%) software development – primarily in Python, (10%) some hardware tasks including, but not limited to PCB design, (15%) collaborative development using git and GitHub.

# Contents

<b>1</b>	<b>Introduction</b>	<b>7</b>
1.1	Literature review . . . . .	7
<b>2</b>	<b>Methodology</b>	<b>12</b>
2.1	Structure of the quadcopter . . . . .	12
2.2	Thrust Overview . . . . .	15
2.3	Quadcopter position manipulation . . . . .	16
2.3.1	Electronic Speed Controllers (ESCs) . . . . .	17
2.3.2	Pitch . . . . .	17
2.3.3	Roll . . . . .	18
2.3.4	Yaw . . . . .	19
2.3.5	IMU (Inertial Measurement Unit) . . . . .	20
2.3.6	Flight controller . . . . .	21
2.4	Control and Estimation . . . . .	21
2.4.1	Quaternions . . . . .	21
2.4.2	Attitude dynamics . . . . .	23
2.4.3	Altitude control . . . . .	23
2.4.4	PD control . . . . .	28
2.4.5	Altitude control system overview . . . . .	30
2.4.6	Simulations . . . . .	31
2.5	Position control (not yet implemented) . . . . .	36
2.5.1	Global positioning to Local positioning . . . . .	36
2.5.2	Modelling . . . . .	37
2.5.3	PID control . . . . .	38
2.5.4	Position control system overview . . . . .	40
2.5.5	Simulations . . . . .	41
<b>3</b>	<b>hardware</b>	<b>44</b>
3.1	Motors . . . . .	44
3.2	Radio . . . . .	45
3.3	Receiver . . . . .	45
3.4	Flight Controller . . . . .	47
3.4.1	Raspberry Pi . . . . .	47
3.4.2	ESP32 . . . . .	48

3.5	Inertial Measurement Unit (IMU) . . . . .	49
3.6	ESC's (Electronic Speed Controller) . . . . .	50
3.7	Propellers . . . . .	50
3.8	Voltage Regulator . . . . .	51
3.9	Battery . . . . .	51
3.10	Sensors . . . . .	52
3.10.1	GNSS Rover Module . . . . .	52
3.10.2	GNSS Base Station . . . . .	53
3.10.3	Base station container and stand . . . . .	54
3.10.4	GNSS Calibration (U-center) . . . . .	54
3.10.5	Time of Flight sensor . . . . .	55
3.10.6	Barometer . . . . .	56
3.10.7	Anemometer . . . . .	56
3.11	Hardware schematic . . . . .	57
3.12	Cost of materials . . . . .	58
3.13	PCB design . . . . .	60
3.13.1	Raspberry Pi PCB . . . . .	60
3.13.2	ESP PCB . . . . .	61
3.13.3	Sensor PCB . . . . .	62
3.13.4	Power Distribution PCB . . . . .	62
<b>4</b>	<b>Software</b> . . . . .	<b>64</b>
4.1	Main Loop . . . . .	65
4.2	Sensor Data Aquisition . . . . .	67
<b>5</b>	<b>Tests</b> . . . . .	<b>69</b>
5.1	GNSS rover rodule test, with correction Vs without . . . . .	69
5.2	Testing of Kalman filter . . . . .	71
5.3	Testing initial estimate for $\alpha_0$ and $\beta_0$ . . . . .	72
5.4	Altitude control . . . . .	73
<b>6</b>	<b>Reflection on progress</b> . . . . .	<b>78</b>
6.1	Time analysis . . . . .	78
6.2	Objective analysis . . . . .	81
6.3	Sustainability . . . . .	83
<b>7</b>	<b>Conclusions</b> . . . . .	<b>85</b>

# Chapter 1

## Introduction

Throughout this project a loitering controller will be designed for the Quadcopter using a GNSS module, time of flight and barometer sensors. The objective of this is to enhance the quadcopters ability to maintain a fixed position in space with high accuracy and minimal drift, this is a challenge in both commercial and civilian quadcopter use.

Loitering technology in quadcopters offers a range of benefits and applications. Security and surveillance, where home/business owners can have real time surveillance, programming a quadcopter to parole specific areas. As well as aerial photography and videography, for those interested in photography or vlogging, quadcopters with loitering capabilities will allow for stable and high-quality aerial shots allowing for anything from time lapse videos to landscape shots.

### 1.1 Literature review

This project will include the development of UAV (Unmanned Aerial Vehicle) technology which will be capable of position hold whilst flying. Throughout the development of this project control algorithms and prediction theory will haе to be researched and implemented.

UAV's as described above have many applications in both commercial and military use. Commercial applications include photography and video [1], home surveillance and security [2], quadcopter light shows [3], agriculture [4] and construction [5]. Some military applications might include disaster management [6], surveillance [7], search and rescue [8].

Due to UAV's wide range of adaptability and use cases it has been researched extensively all around the world. In the study [9] the researchers delve into the specifics of using GPS for location control in quadcopters. Primarily the study focuses on enhancing the accuracy of position holding, they have done this by utilising a way-point system where the quadcopter autonomously navigates through pre-determined points.

The testing which was completed evaluated the quadcopters data supply, GPS sensors used as sensors to determine vehicle coordination points, the LiDAR sensor Lite-V3 is used for measuring altitude. This sensor is accurate up to  $\pm 2.5\text{cm}$  and can read up to 500 values per second, priced around £120.

The waypoints, which were separated into three points at a distance of ten metres each to form a triangular angle; the flights are carried out at 3 waypoints, which are 10 metres each other at a height of five metres; the flights was conducted in the Autonomous mode; the tests were conducted six times. The flight

path was from the home base to waypoint, to waypoint 2, to waypoint 3, all points were 10m apart. The quadcopters system performance was evaluated based on error values between the actual vehicle position and the waypoints coordinates.

They concluded that between waypoint 1 and home the best result they were able to get was 35.8475 cm. between waypoint 1 and 2 the result was 16.2083cm and finally between waypoint 2 and 3 it was 110.2508cm.

Factors to consider for large errors between waypoints that cause the Quadcopter's level of accuracy to not be good are wind speed and inaccurate tuning of the PID controller they were using, this is most prevalent when testing between waypoint 2 and 3. Overall, although there could be improvements, I think the results were good especially in test 2 between waypoint 1 and 2 as they were off by only 16cm.

Furthermore, within this paper there is no evidence of researchers utilising the Kalman filter for position estimation. This would be useful, as if satellite connections were to drop suddenly, the Kalman filter could provide a reliable alternative for estimating the quadcopter's position by fusing readings of the GPS and LiDAR sensors. The Kalman filter, known for its efficiency in dealing with uncertainty and noise in sensor data, could allow for continuous and accurate position tracking even in the absence of GPS signals. This redundancy is crucial for maintaining the stability and safety of the quadcopter during flight, especially in environments where GPS signals are obstructed or non-existent. Incorporating such a filter could significantly enhance the robustness of the control system against signal drop-out, making the quadcopter more reliable for critical applications where consistent positioning is paramount.

The paper presents a detailed study on using GPS technology for the development of an autonomous UAV quadcopter. The GPS module plays a crucial role in outdoor navigation, particularly in altitude stabilization and trajectory mapping for automated flights. The quadcopter uses GPS data for precise positioning and executing flight paths, ensuring stability and accuracy in various outdoor environments.

This study [10] by P. Akademia Baru, S. Sabikan and S. Nawawi emphasizes the integration of GPS in autonomous flight. The GPS facilitates precise positioning, which is paramount for the quadcopter to execute its flight paths accurately. The described precision is not just in horizontal positioning, but it also plays a big part in maintaining a consistent altitude. The GPS data, combined with other on-board sensors, forms a accurate and reliable solution for navigating complex flightpaths in outdoor environments.

Moreover, the paper describes how GPS helps the quadcopter to map out its trajectory, so that the UAV can follow. The waypoints, defined by GPS data, tell the quadcopter which route to take, making it a desirable piece of equipment for manned and unmanned coverage, surveillance, photography, surveying, weather prediction, and search and rescue. GPS-enabled trajectory mapping enables the quadcopter to fly through waypoints, correcting course upon arrival at each node and in mid-course as environmental factors arise, such as wind.

PID control is an important part of quadcopter flight operations, especially in stabilizing flight conditions. This control system adapts the quadcopter's motors based on information provided by the sensors, helping to respond accordingly to environmental changes and operator input. The paper describes the use of PID control in the quadcopter system to ensure good stability in outdoor environments. The PID parameters can be fine-tuned to optimize the response of the quadcopter, increasing overall performance and reliability.

Through testing they also have taken into account the effects high vibrations on the quadcopter and its effect on the accelerometer-based altitude and horizontal position estimates to drift far off from reality. Thus, it will create problems with altitude hold or loiter. To diminish the effects of vibrations they placed the flight controller on an anti-vibration plate, this significantly reduced the vibrations recorded on the IMU. Propeller and motor balancing, however, is also critical for improved performance.

In the second experiment, mission planner software is used to create the flight routes for the quadcopters in advance. They choose to use separate locations for home and land. From WP1 to WP4, five randomly chosen waypoints were added, along with an extra one-second delay. For the duration of the missions, the flight altitude is fixed at 30 metres. The following are the speed settings for waypoint navigation: 700 cm/s for linear speed, 200 cm/s for radius speed, 250 cm/s for speed up rate, 150 cm/s for speed down rate, and 1000 cm/s for loiter speed. This flight mission is conducted six times.

I found that utilising GPS, PID and compass technology they were able to make a quadcopter that was able to follow pre-determined set waypoints with little to no offset furthermore I cannot see any overshoot in and around the waypoints meaning that their PID technology is optimized very well. Overall, this is a great solution for autonomous flying of a quadcopter.

Post analysis of this paper has outlined that if control algorithms were to be utilised in this project it is paramount that they are precisely tuned, the success of the tests in this paper were due to a correctly tuned PID controller allowing for no overshoot.

The paper by Ahmed Hassan Ahmed et al [11] addresses the critical aspect of attitude stabilization and altitude control in quadcopter UAVs, emphasizing the importance of reliable and precise control mechanisms for effective UAV operations. The study initiates with the implementation of a Single Input Single Output (SISO) approach to establish a control structure for a quadcopter using both traditional and modified PID controllers on a single axis, evaluated through key performance metrics such as overshoot and settling time.

A noteworthy contribution of this paper is the comprehensive system architecture it proposes, comprising a flight controller unit, quadcopter system, Inertial Measurement Unit (IMU), and ultrasonic sensor for altitude measurement. The meticulous calibration of the IMU sensors, particularly the accelerometers and gyroscopes, underscores the importance of precise sensor data for accurate UAV control.

The paper looks into the software design aspect, utilising an ARDUINO microcontroller to implement the control algorithms, highlighting the role of digital PID controllers in managing the quadcopter's dynamic movements across pitch, roll, and yaw axes, along with altitude control. This detailed exploration into the control scheme reveals the intricacies involved in achieving stable and responsive UAV flight, especially in the presence of disturbances or added weights that mimic real-world operational challenges.

The MPU-6050 IMU is calibrated by putting it on a level, turntable and positioning each of its three accelerometers, such that its sensitive axes are facing upwards. The average output is recorded after collecting data in this location for roughly 15 minutes. After that, the device is turned so that each sensitive axis is pointing downward, and data is once more gathered for a comparable amount of time to produce an additional average measurement. The sum of these two values, divided by two, to determine the bias for each accelerometer. In order to find the scale factor, the values of each output are subtracted from each other as well as subtracting twice the value of the gravitational acceleration ( $2g$ ), and then dividing the result by twice the gravitational acceleration ( $2g$ ). This process is repeated for each axis to find individual biases and scale factors, ensuring accurate readings from the accelerometers.

Furthermore, the study's experimental setup and implementation of PID controllers on individual axes, followed by a unified control strategy for all axes, provide valuable insights into the practical challenges and considerations in quadcopter control system design. The comparison between traditional and modified PID controllers, in terms of response to disturbances and robustness, adds a layer of depth to the discussion on control system optimization.

From analysing the tests performed, how well the control algorithms are tuned should be noted. In these tests the quadcopter is subjected to disturbance, this is performed by pushing the quadcopter while it is in

position control mode. From graph analysis it is seen that overall the altitude stays consistent with an error of around  $\pm 2$ . When analysing the pitch and roll graphs it is apparent where the quadcopter is exerted to an external force, again the PID controllers have been tuned precisely as they converge within 1 second each time the force is exerted.

In essence, this paper makes a significant contribution to the field of UAV control systems by presenting a well-rounded study on the design, implementation, and evaluation of PID-based control strategies for quadcopter's. It highlights the critical balance between theoretical control system design and practical implementation challenges, offering a valuable resource for researchers and practitioners in the UAV domain.

For implementation on the bzzz quadcopter this paper has highlighted the benefits of PID control algorithms when designing a position control system, as well as information on how to effectively calibrate the IMU. This will be taken into careful consideration when designing the bzzz quadcopter.

In the paper [12] the authors explore the application of reinforcement learning (RL) techniques to improve the control and stability of quadcopters, specifically focusing on altitude holding and path planning. The research is attempting to solve the challenge of maintaining the stability and control of quadcopters in dynamic and uncertain environments, highlighting the need for adaptive and robust control systems.

The study utilises reinforcement learning, with a particular emphasis on Q-learning which is a model-free learning algorithm for controlling the altitude of the quadcopter. The researchers employed PD (Proportional-Derivative) control to stabilize the quadcopter's x and y axes, while the altitude and path planning were managed through the Q-learning algorithm. The training of the quadcopter was conducted in a simulated environment before real-world testing, which is a common practice in RL to minimize risks and costs associated with direct real-world training.

A comparative analysis between the RL approach and a traditional PD algorithm was conducted to evaluate the effectiveness of reinforcement learning in handling the quadcopter's altitude control and path navigation. The paper highlights the potential of RL in improving the quadcopter's performance in navigating through waypoints in an environment with obstacles, formulated as a dimensional grid for the purpose of the study.

One of the key findings of the research is the reinforcement learning algorithm's ability to adapt to unknown environments, demonstrating a more dynamic and flexible approach compared to conventional control methods. The use of Q-learning for path planning showed promising results in avoiding obstacles and reaching designated waypoints, indicating the viability of RL in complex navigation tasks.

However, the paper also discusses the limitations and challenges associated with the implementation of RL in quadcopters, such as the computational complexity of the learning algorithm and the need for extensive training data to achieve optimal performance. The authors suggest future work could explore the integration of continuous state spaces and the application of deep learning techniques to enhance the learning process and efficiency of the quadcopter's control system.

Overall, the study contributes to the growing developments in reinforcement learning in UAVs (Unmanned Aerial Vehicles), offering insights into the potential benefits and challenges of integrating advanced machine learning techniques into quadcopter technology for improved autonomy and performance in aerial tasks.

In conclusion, the studies emphasises how crucial it is to design a quadcopter control system for the bzzz quadcopter. PID control mechanisms contribute to accuracy and stability, this will be a crucial component in the design of the bzzz quadcopters. furthermore it is highlighted how important it is to fine-tune PID controllers in order to minimise overshoot and provide accurate reactions to changes in the environment. The UAV's ability to retain its planned course during intricate manoeuvres with few errors is dependent on

this tuning process, which is crucial for the quadcopter’s success in applications such as photography [1].

Additionally, the bzzz quadcopter will integrate Kalman filters to enhance reliability in GPS-denied environments as indicated in existing literature. This integration aims to strengthen the UAV against signal disruptions, ensuring continuous operation, and enhancing safety—crucial considerations for tasks like disaster management [6] and search and rescue operations [8].

Although reinforcement learning shows promising advancements, this technology will not be utilised in the current version of the bzzz quadcopter due to its complexity and extensive data requirements that do not align with the project’s current objectives [12]. Instead, our main goal is to refine the PID controllers and Kalman filters to create a precise control system that meets the requirements of operating the bzzz quadcopter. This targeted approach ensures the deployment of a robust UAV platform, ready to excel across a spectrum of applications with proven technology that balances performance with operational feasibility.

# Chapter 2

## Methodology

### 2.1 Structure of the quadcopter

The quadcopter we have designed has an X configuration where each motor lies at the corner of the quadcopter and one side acts as the front of the quadcopter depicted below (Fig.2.1).



Figure 2.1: Bzzz quadcopter

The quadcopter is shaped like an 'X,' with each arm extending diagonally from the center body, where the core components are housed. Here's a detailed overview of its structure:

## Frame



Figure 2.2: Central hub attached to the arms

- **The Central Hub**, the quadcopter's central hub, houses vital parts required for its functionality, making it crucial to its operation. The battery compartment is positioned inside this core in a way that maximises the quadcopter's centre of gravity and promotes steady and balanced flight dynamics. Mounting plates are essential for the quadcopter's operational capabilities and versatility as they offer safe attachment points for structural components like landing gear. Moreover, the landing gear attachments' direct integration into the hub allows for seamless and secure operations while strengthening the structure to withstand the stresses of take-off and landing. The arrangement of parts inside the central hub improves the quadcopter's performance and manoeuvrability in addition to preserving its structural integrity.
- **The Arms**, four arms extend out of the central hub in an X configuration, this is where the motor housings are fastened, these housings are designed to accommodate the quadcopter's motors, protecting them from damage while ensuring they remain firmly attached, even under the stress of high-speed rotation and the various forces experienced during flight manoeuvres. As well as the propeller guards, These guards serve as a protective barrier around the spinning propellers, safeguarding against accidental contact with objects or people. The guards help to prevent damage to the propellers and reduce the risk of injury from the spinning blades.

## Landing gear



Figure 2.3: Quadcopter legs feet and dampers

- **Quadcopters legs**, the four quadcopter legs are all the same length and run parallel to the arms from the central hub towards the ground. These stands are responsible for keeping the quadcopter horizontal for a smooth take off and landing. The stands also provide necessary clearance between the quadcopter's body (and potentially any attached components or sensors) and the ground. This clearance is important to prevent damage to the underside of the quadcopter and any sensitive equipment during landing or when taking off from uneven terrain.
- **Feet and Dampers**, the black feet which are fastened to the bottom of the stands ensure that the foam dampers are security fastened onto the bottom of the quad, taking a horse shoe like shape which matches the shape of the dampers. The dampers absorb the impact when the quadcopter lands. This helps protect the integrity of the frame and sensitive components from the shock and vibration that occur during landing, especially on hard or uneven surfaces. They are also used to reduce vibrations transmitted from the ground to the quadcopter's frame during landing and takeoff. By dampening these vibrations, the foam contributes to more stable take off and landings and helps protect onboard components.

## Electronic housing



Figure 2.4: Electronic Housing

The white caged electronic housing box is where the computational unit, an Inertial Measurement Unit (IMU), Raspberry Pi, Radio receiver, GNSS rover module and voltage regulator are all placed at the center of the body, situated above the central hub. For more information on the electronic components used please see section....

## 2.2 Thrust Overview

This section briefly runs over how the quadcopter produces thrust. A quadcopter uses four separate brushless (BLDC) motors, each paired with a specific electronic speed controllers (ESCs) that adjusts how fast the motor spins. These controllers work by receiving a digital signal, known as Pulse-Width Modulation (PWM) which have a pulse, the 'width' of these pulses (i.e., how long they stay 'on' versus 'off' in a given cycle) is adjusted to control the speed of the motor. This is known as the duty cycle. A longer 'on' time (wider pulse) means more power is delivered to the motor, making it spin faster. Digital microcontrollers are typically used to create these PWM signals.

Propellers generate thrust through aerodynamic principles, primarily by leveraging the pressure differential created by the airfoil-shaped blades as they slice through the air. According to Bernoulli's principle, the acceleration of air over the blade surfaces leads to a lower pressure on the top side compared to the bottom, due to the faster flow of air this pressure difference produces lift. This is a similar concept to an aircraft wing. Furthermore, Newton's third law of motion: every action has an equal and opposite reaction, should be considered as the propeller blades push air downwards, resulting in an upward reactionary force. The efficiency of this process is influenced by the propeller's angle of attack and the rotational speed, which determine the volume of air displaced. However, factors such as viscous drag and turbulence can reduce the thrust efficiency, necessitating aerodynamic optimizations to minimize energy losses and maximise the generated thrust, see Fig.2.6.

On the quadcopter depicted in Fig.2.1 and Fig.2.5 two motors spin in a clockwise direction and two in the anticlockwise direction, motors which rotate in the same direction are placed on opposite sides of the diagonal arms. The reason for this is to provide stability and accurate control. By counteracting the

angular momentum produced by each motor, this arrangement keeps the quadcopter oriented and stops it from spinning out of control. The quadcopter's stability is enhanced by the deliberate positioning of motors rotating at the same speed on opposing diagonal arms, which balances torque. Additionally, by adjusting the motors' rotational speeds, this configuration makes it easier to perform yaw motions, which are necessary for steering and adjusting orientation on the x-axis. This design decision improves manoeuvrability and simplifies the entire structure, removing the need for more intricate programming to resist rotating forces. As a result, the control system becomes simpler and more effective through the use of the ESC's.

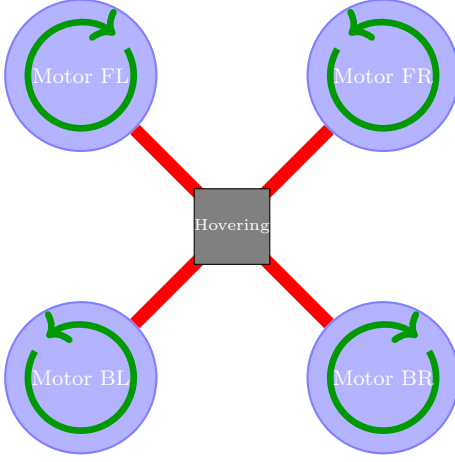


Figure 2.5: Motor configuration top view.

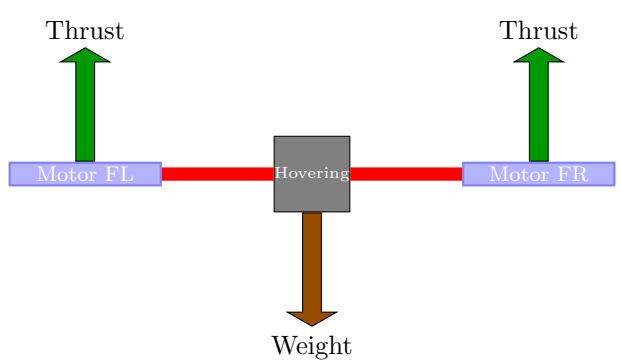


Figure 2.6: Side view of a quadcopter with motor thrust.

As we can see from the above diagrams in Fig.2.5 and Fig.2.6, the motors are spinning at a rate at which the thrust produced is greater than the weight of the quadcopter, allowing it to hover. The direction of the thrust arrows in the diagrams indicates the rotation of each propeller allowing a force exerted by each motor to counteract gravity and maintain the quadcopter's hovering state. The balanced forces from opposite motors, as depicted in the top view (Fig.2.5), ensure stability and control, while the side view (Fig. 2.6) illustrates how the collective thrust from all motors must exceed the downward force of the quadcopter's weight to achieve lift. This equilibrium between thrust and weight is essential for the quadcopter to remain airborne and perform various manoeuvres.

Please note that the diagrams produced are not to scale and are just for the readers understanding on how the quadcopters thrust dynamics are produced.

## 2.3 Quadcopter position manipulation

In this section we will go through the quadcopters dynamics and how we can manipulate them in order to manoeuvre the quad to achieve a specified position and or direction of flight

1. **Pitchx**, measured around a body fixed x-axis.
2. **Roll**, measured around a body fixed y-axis.
3. **Yaw** or heading, measured along a body fixed z-axis.

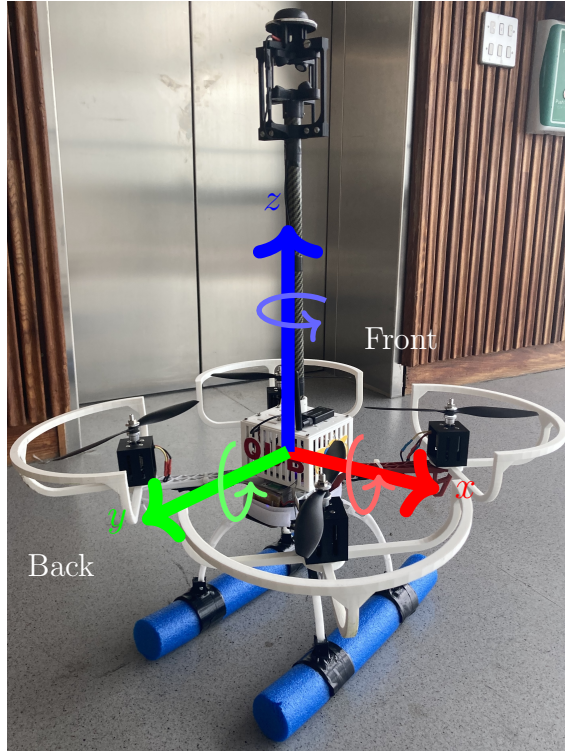


Figure 2.7: Quadcopter with pitch, roll and yaw axes.

### 2.3.1 Electronic Speed Controllers (ESCs)

Electronic Speed Controllers (ESCs) precisely control the speed of each rotor, enabling pilots to execute complex pitch roll and yaw manoeuvres and retain stability, even in challenging conditions. This is accomplished by computing the difference in velocity that controls the rate of rotation between pairs of rotors spinning clockwise and anticlockwise on every axis.

### 2.3.2 Pitch

Pitch control in a quadcopter is achieved through the manipulation of the rotational speeds of its rotors (FL, FR, BL, BR Fig.2.5), which in turn alters the thrust produced by each motor. To initiate a pitch movement, which is a forward or backward tilt leading to forward or backward movement, the quadcopter adjusts the speed of its front and rear rotors relative to each other.

To initiate a forward pitch, the rear rotors (BL and BR) are amplified to produce additional lift at the back of the quadcopter. At the same time, decelerating the front rotors reduces their lifting capacity in turn leading to an uneven force distribution along x-axis which causes movement towards the front direction as the thrust produced by the back motors is greater than that of the front, this leads to a positive torque. Conversely, when executing a backward pitch manoeuvre on a quadcopter, the front rotors (FL and FR) rotate at an accelerated pace while the rear ones slow down, as the thrust produced by the front motors is greater than that of the back, this leads to a negative torque on the x-axis. This disparity in speed results in the unmanned aerial vehicle leaning backwards.

The resulting torque produced on the x-axis is shown below:

$$\tau_{x,total} = \frac{d}{\sqrt{2}}(T_{FL} + T_{FR} - T_{BL} - T_{BR}) \quad (2.1)$$

Where,  $T_{FL}$ ,  $T_{FR}$ ,  $T_{BL}$  and  $T_{BR}$  are forces of thrust by the motors, d is the distance of the center of mass from any one motor (length of the quadcopters arm).

The torque calculation is affected by the leverage effect of the motor thrusts, namely the perpendicular distance between the centre and the line of action of each motor's thrust. Because the perpendicular distance in a square arrangement is smaller than the diagonal by a factor of  $\sqrt{2}$ , the torque formula divides by  $\sqrt{2}$ .

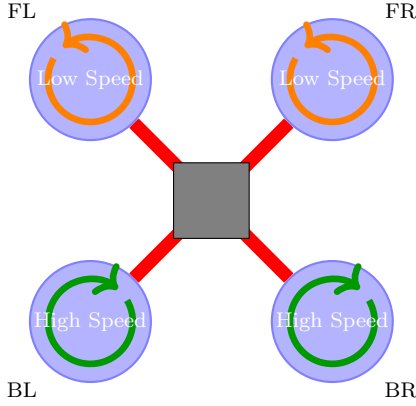


Figure 2.8: Illustration of forward pitch on quadcopter

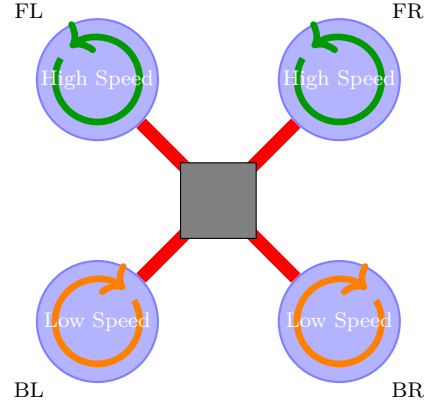


Figure 2.9: Illustration of backward pitch on quadcopter

Figure 2.8 illustrates a pitch to the front of the quadcopter, motors BL and BR are spinning faster than FL and FR. This leads to more thrust being produced by the back two motors than the front two. This causes the quadcopter to rotate in a clockwise motion along the x-axis.

On the other hand Figure 2.9 illustrates a pitch to the back of the quadcopter, motors FL and FR are spinning faster than BL and BR. This leads to more thrust being produced by the front two motors than the back two. This causes the quadcopter to rotate in an anti-clockwise motion along the x-axis.

### 2.3.3 Roll

To manoeuvre the quadcopters roll, adjusting the speeds of its rotors is key. This involves creating an imbalance in thrust between either side of the aircraft prompting it to tilt along its y-axis depicted in Fig.2.7. When initiating a roll to the right side the quadcopter increases the speed of its left side rotors (FL and BL) while decreasing that of its right side rotors (FR and BR). This disparity in thrust causes a torque that tilts and rolls it to the right. Conversely, for a roll the opposite occurs the quadcopter increases the speed of its right side rotors (FR and BR) while decreasing that of its left side rotors (FL and BL). Through the use of roll the quadcopter adjusts its orientation and gains movement in that direction.

The resulting torque produced on the y-axis is shown below:

$$\tau_{y,total} = \frac{d}{\sqrt{2}}(T_{FL} + T_{FR} - T_{BL} - T_{BR}), \quad (2.2)$$

where,  $T_{FL}$ ,  $T_{FR}$ ,  $T_{BL}$  and  $T_{BR}$  are forces of thrust by the motors, d is the distance of the center of mass

from any one motor (length of the quadcopters arm).

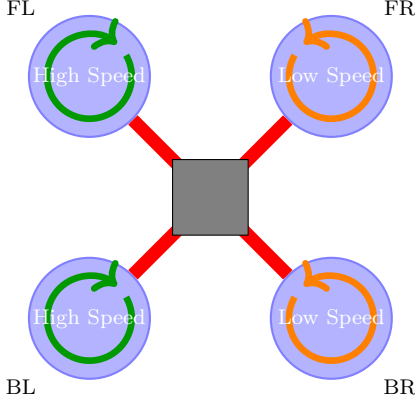


Figure 2.10: Illustration of right roll on quadcopter

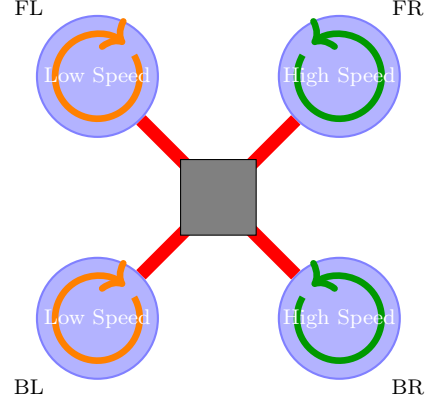


Figure 2.11: Illustration of left roll on quadcopter

Figure 2.10 illustrates a roll to the right of the quadcopter, motors FL and BL are spinning faster than FR and BR. This leads to more thrust being produced by the two left motors than the two right. This discrepancy in thrust causes the quadcopter to rotate in a clockwise motion along the y-axis.

On the other hand Figure 2.11 illustrates a roll to the left of the quadcopter, motors FR and BR are spinning faster than FL and BL. This leads to more thrust being produced by the two right motors than the two left motors. This discrepancy in thrust causes the quadcopter to rotate in an anti-clockwise motion along the y-axis.

### 2.3.4 Yaw

By adjusting rotor speeds, one may precisely control a quadcopter's yaw, or rotation about the vertical z-axis (see Fig.2.7). To do this, opposing diagonal rotors must rotate at different speeds in order to produce torque, which causes rotation around the vertical axis.

The quadcopter rotates clockwise when viewed from above, it achieves this by increasing the speed of the counter-clockwise (FL and BR) and reducing the speed of the clockwise (FR and BL) (Fig.2.5) spinning rotors. This generates positive (upward) torque that turns it to the right. this torque can be represented by  $\tau_{cw}$ .

Similar adjustments are performed to the rotor speeds for an anticlockwise or leftward movement: FR and BL spin more quickly as FL and BR slow down, generating an overall negative (downward) torque  $\tau_{acw}$  causing the quadcopter to turn to the left.

The resultant torque of the overall model from can be given by:

$$\tau_{z,total} = \tau_{acw} - \tau_{cw} \quad (2.3)$$

The direction of motion can be determined from torque by using, the Right-Hand Rule: Point your right hand's fingers in the direction of the position vector (from the axis of rotation to the point where force is applied). Curl them toward the direction of the force. Your thumb points in the direction of the torque vector. If your thumb points out of the page (towards you), the torque is anti-clockwise (acw), leading to anti-clockwise motion. If your thumb points into the page (away from you), the torque is clockwise (cw), leading to clockwise motion.

Expanding on the idea of using torque to determine motion direction, it's vital to acknowledge that a system comprising several motors (FL, FR, BL, BR) can have its total torque analysed by breaking the system down into individual torques generated by each motor. The sum of the individual reaction torques produced by each motor is represented in the Equation below.

$$\begin{bmatrix} \tau_{acw} \\ \tau_{cw} \end{bmatrix} = \begin{bmatrix} \tau_{FL} + \tau_{BR} \\ \tau_{FR} + \tau_{BL} \end{bmatrix} \quad (2.4)$$

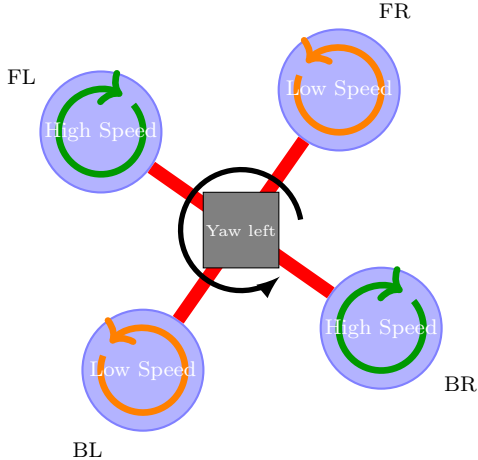


Figure 2.12: Illustration of acw yaw on quadcopter

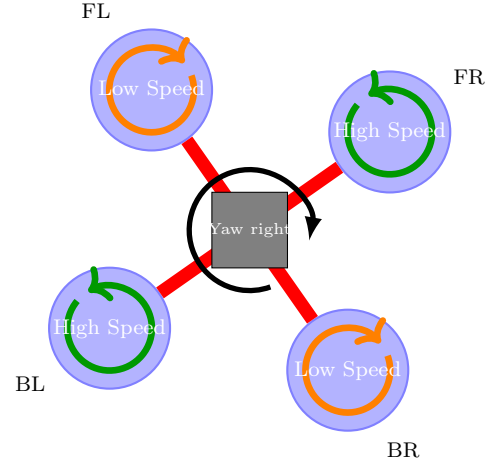


Figure 2.13: Illustration of cw yaw on quadcopter

In both of the above diagrams Fig.2.12 and Fig.2.13 show the cw and acw yaw mechanics. Fig.2.12 shows a yaw to the left, this is due to the fact that motors, FL and BR are running faster than the motors FR and BL this produces a positive total torque as a result of equation 2.3, this in turn, will cause the quadcopter to yaw in an anti-clockwise direction (to the left).

Conversely, Fig.2.13 shows a yaw to the right, this is due to the fact that motors, FR and BL are running faster than the motors FL and BR this produces a negative total torque as a result of equation 2.3, this in turn, will cause the quadcopter to yaw in a clockwise direction (to the Right).

Finally when all motors spin at the same rate the resultant total torque ( $\tau_{total}$ ) is zero, resulting in the quadcopter staying stationary.

Ultimately, Pitch, Roll and Yaw processes work together seamlessly to enhance the quadcopters manoeuvrability during flights for more accurate adjustments in orientation as required throughout each journey.

### 2.3.5 IMU (Inertial Measurement Unit)

An Inertial Measurement Unit (IMU) is a crucial part of electronics that combines a magnetometer, accelerometer, and gyroscope. The accelerometer measures changes in velocity along linear axes in metres per second squared, while the gyroscope tracks rotational motion in degrees per second and finally, the magnetometer measures magnetic field strength in micro-Teslas. Through the use of an advanced digital filter such as the Madgwick filter, the IMU is able to precisely determine the orientation of the quadcopter. Using the IMU in this way guarantees accurate orientation data, which is essential for quadcopter applications. More details into the IMU which is being used can be seen below (see Section:3.5)

### 2.3.6 Flight controller

Controlling the pitch roll and yaw motions of the quadcopter is a crucial responsibility of the flight controller. It processes the IMU data to understand the vehicle's orientation and motion, then makes decisions to adjust the motors and stabilize the flight. For more information on the flight controller see Section:3.4

## 2.4 Control and Estimation

During this project the development of a kalman filter for position estimation on the z-axis was paramount for sensor fusion. On the quadcopter there is a downward-facing time-of-flight (ToF) sensor, which is an infrared distance sensor that measures the distance from the ground with a standard error of  $\pm 6$  cm. The quadcopter carries a barometer which by measuring the barometric pressure can give an estimate of the altitude (where the altitude is zero at sea level); the standard error of this sensor is  $\pm 25$ cm. The quadcopter is also equipped with a GNSS (global navigation satellite system) sensor, which uses the ZED-FP9 module. The GNSS module is coupled with a base GNSS station, which allows it to produce accurate position estimates. The GNSS can estimate the altitude of the vehicle (with respect to the sea level) with a standard error of  $\pm 5$  cm. for more information on the sensors used see Section:3.

### 2.4.1 Quaternions

Building on the foundational principles of pitch, yaw, and roll seen in Section2.3, the system dynamics of a quadcopter extend into the realm of intricate motion control and stability mechanisms. A typical quadcopter can manoeuvre on any axis fixed to its frame, it can ascend or descend vertically, and move laterally in the (x, y) plane of a known global reference frame. The quadcopter's ability to move in a variety of ways enables it to precisely navigate aerial waypoints, adapting seamlessly to both the immediate environment and the pilot's commands.

A quaternion is a mathematical entity that extends complex numbers, characterized by a four-dimensional vector space. It can be depicted through various notations; the following expressions illustrate two commonly recognised methods. The operation of quaternion multiplication is inherently non-commutative, mirroring the nature of rotational operations. The components of a quaternion labelled as  $q_1$  to  $q_3$  constitute its vector component, whereas  $q_0$  serves as its scalar component. As seen below,

$$q = q_0 + q_1 i + q_2 j + q_3 k \quad (2.5)$$

$$q = [q_0 + q_1 + q_2 + q_3]^T \quad (2.6)$$

The elements  $i, j$  and  $k$  satisfy the properties  $i^2 = j^2 = k^2 = ijk = -1$ . A quaternion with a norm equal to 1 this can be used to represent a rotation of the quadcopter. Specifically, one can express a unit quaternion with the formula  $q = \cos\left(\frac{\theta}{2}\right) + (i\hat{n}_x + j\hat{n}_y + k\hat{n}_z)\sin\left(\frac{\theta}{2}\right)$ , depicting a rotational transformation about the unit vector  $\hat{n} = (\hat{n}_x, \hat{n}_y, \hat{n}_z)$  through an angle  $\theta$ . By conversion, the quaternion  $e = 1 + 0i + 0j + 0k$  denotes the identity rotation, signifying no change in orientation, aligned with the standard orientation of the quadcopter.

The multiplication of two quaternions, labelled as  $p$  and  $q$ , is executed through the Kronecker product, denoted by  $\otimes$ . The resulting quaternion is outlined in the equations that follow. When  $p$  is associated with a specific rotation and  $q$  with another, the product  $p \otimes q$  yields the resultant rotation combining both. It is

pivotal to highlight that the multiplication process for quaternions is inherently non-commutative, mirroring the non-commutative characteristic of rotations themselves. The bilinear operation  $p \otimes q$  is equal to the matrix  $Q(p)q$  as seen below:

$$p \otimes q = \begin{bmatrix} p_0 & -p_1 & -p_2 & -p_3 \\ p_1 & p_0 & -p_3 & p_2 \\ p_2 & p_3 & p_0 & -p_1 \\ p_3 & -p_2 & p_1 & p_0 \end{bmatrix} \begin{bmatrix} q_0 \\ q_1 \\ q_2 \\ q_3 \end{bmatrix} \quad (2.7)$$

equivocally,

$$q \otimes p = \begin{bmatrix} q_0 & -q_1 & -q_2 & -q_3 \\ q_1 & q_0 & q_3 & -q_2 \\ q_2 & -q_3 & q_0 & q_1 \\ q_3 & q_2 & -q_1 & q_0 \end{bmatrix} \begin{bmatrix} p_0 \\ p_1 \\ p_2 \\ p_3 \end{bmatrix} \quad (2.8)$$

Normalizing a quaternion ensures its magnitude (or norm) remains equal to one, which is crucial for maintaining the quaternion's representation of rotation. A normalized quaternion  $q$  can be obtained by dividing the quaternion by its norm, where the norm  $\|q\|$  is defined as:

$$\|q\| = \sqrt{q_0^2 + q_1^2 + q_2^2 + q_3^2}. \quad (2.9)$$

The conjugate of a quaternion  $q = q_0 + q_1i + q_2j + q_3k$  is given by:

$$q^* = q_0 - q_1i - q_2j - q_3k. \quad (2.10)$$

similarly,

$$q^* = [q_0 - q_1 - q_2 - q_3]^\top \quad (2.11)$$

The inverse  $q^{-1}$  of a unit quaternion is equal to its conjugate over its norm squared:

$$q^{-1} = \frac{q^*}{\|q\|^2} \quad (2.12)$$

This property simplifies the computation of the inverse for unit quaternions and is particularly useful in rotational transformations.

Quaternions are extensively used in the stabilization and control of quadcopters. For instance, the desired rotation  $q_d$  can be achieved by applying a control torque  $\tau$  based on the error between the desired and current quaternion  $q$ :

$$\tau = -K_p(q \otimes q_d^* - 1) - K_d\dot{q}, \quad (2.13)$$

where  $K_p$  and  $K_d$  are the proportional and derivative gains,  $q \otimes q_d^*$  calculates the quaternion error by determining the rotation from the desired orientation to the current orientation. One in the equation represents the quaternion identity, which signifies no rotation, respectively.

For deeper insights into quaternion mathematics and its applications in aerospace and robotics, consider exploring the following resources [13] [14] [15]

## 2.4.2 Attitude dynamics

Attitude dynamics refers to the study and control of the orientation and rotation of the quadcopter as it moves through the air. It encompasses understanding how the quadcopter's attitude (its orientation with respect to an inertial frame of reference, usually the Earth) changes in response to various forces and moments applied to it. Furthermore, how to control these changes to achieve desired orientations and flight paths.

The attitude dynamics of the quadcopter are modelled by two quaternion dynamic equations:

$$\dot{q} = \frac{1}{2} \otimes q \begin{bmatrix} 0 \\ \omega \end{bmatrix}, \quad (2.14)$$

$$\dot{\omega} = I_{cm}^{-1} \cdot \tau - I_{cm}^{-1} [\omega \times (I_{cm} \cdot \omega)] \quad (2.15)$$

Equation(2.14) uses quaternions to handle the orientation of the quadcopter in 3D space. Quaternions are an alternative to Euler angles and avoid the problem of gimbal lock, making them favourable for applications like quadcopter control where orientation needs to be tracked continuously and smoothly.  $\dot{q}$  represents the time derivative of the quaternion, essentially describing how the orientation changes over time,  $q$  represents the current orientation of the quaternion equation and  $\omega$  is the angular velocity vector of the quadcopter taken from the IMU around  $(x, y, z)$  respectively.

Equation(2.15) describes how the angular velocity ( $\omega$ ) of the quadcopter changes over time, denoted by  $\dot{\omega}$ .  $I_{cm}$  is the moment of inertia matrix, which describes how the mass of the quadcopter is distributed relative to the center of mass (cm) around each of its axes and  $I_{cm}^{-1}$  is the inverse of the moment of inertia matrix, which is used to calculate the angular acceleration from the applied torques ( $\tau$ ).

Both equations((2.14)) and ((2.15)) were derived and changed from [15]

## 2.4.3 Altitude control

The altitude dynamics of a quadcopter are defined within a global coordinate system, crucial for maintaining a predetermined altitude from the Earth's surface. The model that describes these dynamics is based on fundamental principles, delineated as follows:

The rate of change of the quadcopter's altitude, represented as  $\dot{z}_t$ , is the result of the vertical acceleration  $a_{T_t}^z$  produced by the quadcopter's motors at a given time minus the gravitational acceleration,  $g$ . This equation is continuous in time and is expressed as,

$$\dot{z}_t = a_{T,t}^z - g \quad (2.16)$$

Here,  $a_{T_t}^z$  signifies the upward acceleration generated by the propulsion at time  $t$ , measured in meters per second squared. The constant  $g$  denotes the acceleration due to Earth's gravity, also in meters per second squared. The altitude  $z_t$  represents the quadcopter's center of mass's vertical position at time  $t$ , measured in meters.

Additionally, the quadcopter's vertical velocity  $v_{z_t}$  and vertical acceleration  $a_{z_t}$  are defined by the rate of altitude change  $\dot{z}_t$  and the rate of vertical acceleration change  $\dot{a}_{T_t}^z - g$ , respectively. The term  $\dot{a}_{T_t}^z$  is derived from the quadcopter's upward thrust and serves as the system's input, while  $g$  is considered a constant input in the opposite direction.

Let  $y_t^z = z_t$  be the output equation of the system.

## Modelling

The two main forces acting on the quadcopter are the weight,  $mg$ , and the force from the propellers,  $F_{\text{prop}}$ , which has been found to depend linearly on the throttle reference signal  $\tau \in [0, 1]$ . The throttle reference signal is a signal that is sent to the electronic speed controllers (ESCs) of the four motors; at  $\tau = 0$  the motors do not spin, whereas  $\tau = 1$  corresponds to the maximum rotation speed.

In an experiment, the quadcopter was placed on digital scales and the lift (in g) was measured for different values of  $\tau$ . The experimental results are shown in Figure 2.14, from which it seems that a reasonable model for the lifting force is

$$F_{\text{prop}} = \alpha_0\tau + \beta_0, \quad (2.17)$$

where  $\alpha_0 > 0$  and  $\beta_0 < 0$  are constants, which depend on the level of charge of the battery. Although the values of  $\alpha_0$  and  $\beta_0$  can be estimated from the data shown in Figure 2.14, their exact value is unknown while flying.

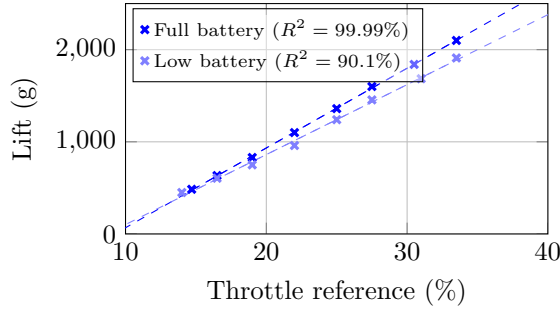


Figure 2.14: Static lift (g) plotted against throttle reference (%).

From the model of Equation (2.17), the total acceleration is

$$a = \frac{F_{\text{prop}} - mg}{m} = \frac{\alpha_0\tau + \beta_0 - mg}{m} = \frac{\alpha_0}{m} + \frac{\beta_0 - mg}{m} = \alpha\tau + \beta, \quad (2.18)$$

where,

$$\alpha = \alpha_0/m \quad (2.19)$$

and

$$\beta = (\beta_0 - mg)/m \quad (2.20)$$

As a result, a dynamical model of the system is

$$\ddot{z} = a \Leftrightarrow \ddot{z} = \alpha\tau + \beta, \quad (2.21)$$

where  $z$  denotes the altitude of the quadcopter. Note again, that the exact values of the coefficients  $\beta$  and  $\alpha$  are not known while flying (but we will estimate them). We can write this model as

$$\dot{z} = v, \quad (2.22a)$$

$$\dot{v} = \alpha\tau + \beta, \quad (2.22b)$$

where  $v$  is the quadcopter's vertical velocity. By discretising, using Euler's discretisation, with sampling

time  $T_s$ , we have

$$z_{t+1} = z_t + T_s v_t. \quad (2.23a)$$

$$v_{t+1} = v_t + T_s(\alpha\tau_t + \beta). \quad (2.23b)$$

The sampling time is  $T_s = 100$  ms. Note that this system is at equilibrium whenever  $\alpha\tau_t + \beta = 0$ , that is, equivalently,  $\tau_t = -\beta/\alpha$ . This defines the *hovering throttle signal*,  $\tau^{\text{eq}} = -\beta/\alpha$ .

## Estimator Design

### State Vector Definition

The state vector  $x_t$  is defined as,

$$x_t = [z_t \ v_t \ \beta_t \ \alpha_t \ d_t^{\text{bar}} \ d_t^{\text{Tof}}] \quad (2.24)$$

in order to compute the throttle signal  $\theta$  values for  $z, v, \alpha$  and  $\beta$  need to be estimated. These measurements often are subject to noise, therefore the system dynamics are seen below,

$$z_{t+1} = z_t + T_s v_t + w_t^z \quad (2.25)$$

$$v_{t+1}^z = v_t^z + T_s(\alpha_t \tau_t + \beta_t) + w_t^v \quad (2.26)$$

$$\beta_{t+1} = \beta_t + w_t^\beta, \quad (2.27)$$

$$\alpha_{t+1} = \alpha_t + w_t^\alpha. \quad (2.28)$$

$$(2.29)$$

We define  $w_t^z$  and  $w_t^v$  as the process noise elements.  $w_t^z$  is distributed normally with zero mean and variance  $\sigma_z^2$ , expressed as  $w_t^z \sim \mathcal{N}(0, \sigma_z^2)$ , and similarly,  $w_t^v$  follows a normal distribution with  $w_t^v \sim \mathcal{N}(0, \sigma_v^2)$ . Additionally,  $w_t^\alpha$  and  $w_t^\beta$  represent white noise processes with distributions  $w_t^\alpha \sim \mathcal{N}(0, T_s \sigma_\alpha^2)$  and  $w_t^\beta \sim \mathcal{N}(0, T_s \sigma_\beta^2)$  respectively. The system state to be estimated is denoted by  $x_t = (z_t, v_t^z, \alpha_t, \beta_t)$ , with the state update equation  $x_{t+1}$  defined as,

$$x_{t+1} = A_t x_t, \quad (2.30)$$

### State transition matrix $A_t$

The state transition matrix  $A$  describes how the state at time  $t$  evolves to the state at time  $t + 1$ . For the given system. Given the state vector  $x_t = [z_t \ v_t^z \ \alpha_t \ \beta_t \ d_{\text{bar}} \ d_{\text{Tof}}]$  (2.24) and output  $y_t = [y_t^{\text{gnss}} \ y_t^{\text{ToF}} \ y_t^{\text{bar}}]$ , the state transition matrix  $A_t$  from the system's dynamic model is defined as:

$$A_t = \begin{bmatrix} 1 & T_s & 0 & 0 & 0 & 0 \\ 0 & 1 & T_s \tau_t & T_s & 0 & 0 \\ 0 & 0 & 1 & 0 & 0 & 0 \\ 0 & 0 & 0 & 1 & 0 & 0 \\ 0 & 0 & 0 & 0 & 1 & 0 \\ 0 & 0 & 0 & 0 & 0 & 1 \end{bmatrix} \quad (2.31)$$

where  $T_s$  is the sampling time, and  $\tau_t$  represents the throttle signal at time  $t$ .

$$x_{t+1} = \begin{bmatrix} 1 & T_s & 0 & 0 & 0 & 0 \\ 0 & 1 & T_s \tau_t & T_s & 0 & 0 \\ 0 & 0 & 1 & 0 & 0 & 0 \\ 0 & 0 & 0 & 1 & 0 & 0 \\ 0 & 0 & 0 & 0 & 1 & 0 \\ 0 & 0 & 0 & 0 & 0 & 1 \end{bmatrix} x_t + w_t \quad (2.32)$$

### Process Noise Covariance Matrix $Q$

The process noise covariance matrix  $Q$  represents the covariance of the process noise, accounting for the uncertainty in the model dynamics:

$$Q = \begin{bmatrix} \sigma_z^2 & 0 & 0 & 0 & 0 & 0 \\ 0 & \sigma_v^2 & 0 & 0 & 0 & 0 \\ 0 & 0 & T_s \sigma_\alpha^2 & 0 & 0 & 0 \\ 0 & 0 & 0 & T_s \sigma_\beta^2 & 0 & 0 \\ 0 & 0 & 0 & 0 & \sigma_{d_{ToF}}^2 & 0 \\ 0 & 0 & 0 & 0 & 0 & \sigma_{d_{bar}}^2 \end{bmatrix} \quad (2.33)$$

Here,  $\sigma_z^2$ ,  $\sigma_v^2$ ,  $\sigma_\alpha^2$ ,  $\sigma_\beta^2$ ,  $\sigma_{d_{ToF}}^2$  and  $\sigma_{d_{bar}}^2$  represent the variances of the altitude, velocity, and the coefficients  $\alpha$  and  $\beta$ , which relate the throttle signal to the lift.

### Outputs

The output  $y$  is shown by the following,

$$y = [y^{gnss}, y^{ToF}, y^{bar}] \quad (2.34)$$

for the barometer sensor's output, denoted by  $y_{bar}$ , is described by the equation,

$$y^{bar} = z + d^{bar} + w^{bar} \quad (2.35)$$

where,

$$d_{t+1}^{bar} = d_t^{bar} + w_t^{bar} \quad (2.36)$$

The bias ( $d^{bar}$ ) should stay consistent throughout readings, the second reading of the bias should be equal to the first allowing for some additional noise/offset.

For the GPS (GNSS module) sensor's output, denoted by  $y^{gnss}$ , is described by the equation,

$$y^{gnss} = z + w^{gnss} \quad (2.37a)$$

The Time-of-Flight (ToF) sensor's output, denoted by  $y^{ToF}$ , is described by the equation, which is equal to the altitude plus a bias term plus the measurement noise; overall,

$$y^{ToF} = z + d^{ToF} + w^{ToF} \quad (2.38)$$

where we assume that  $d^{tof}$  is described by a simple model of the form t

$$d_{t+1}^{tof} = d_t^{tof} + w_t^{tof} \quad (2.39)$$

Through all sensors  $y$  represents the output from the sensor. The variable  $z$  signifies the quadcopter's altitude, which is the measurement for all sensors. The term  $w$  encapsulates the measurement noise or errors associated with the sensors. This noise term,  $w$ , encompasses various factors such as sensor inaccuracies, the impact of environmental conditions on sensor performance, and any systematic bias that might be inherent in the sensor's readings.

### Measurement Matrix $C$

The measurement matrix  $C$  links the state vector to the measurement vector:

$$C = \begin{bmatrix} 1 & 0 & 0 & 0 & 0 & 0 \\ 1 & 0 & 0 & 0 & 0 & 1 \\ 1 & 0 & 0 & 0 & 1 & 0 \end{bmatrix} \quad (2.40)$$

This matrix considers the direct measurement of altitude by all sensors and accounts for biases in the ToF and barometer sensors. Were the first row represents the GNSS sensor, the second represents the ToF and the third represents the barometer

The measurement model is defined as

$$y_t = Cx_t + w_t \quad (2.41)$$

$$y_t = \begin{bmatrix} 1 & 0 & 0 & 0 & 0 & 0 \\ 1 & 0 & 0 & 0 & 0 & 1 \\ 1 & 0 & 0 & 0 & 1 & 0 \end{bmatrix} x_t + w_t \quad (2.42)$$

where,  $y_t$  is the current update.

### Measurement Noise Covariance Matrix $R$

The measurement noise covariance matrix  $R$  accounts for the uncertainty in sensor measurements:

$$R = \begin{bmatrix} \sigma_{gnss}^2 & 0 & 0 \\ 0 & \sigma_{ToF}^2 & 0 \\ 0 & 0 & \sigma_{bar}^2 \end{bmatrix} \quad (2.43)$$

where  $\sigma_{bar}^2$ ,  $\sigma_{gnss}^2$ , and  $\sigma_{ToF}^2$  are the variances of the measurement noises for the barometer, GPS, and Time-of-Flight sensors, respectively.

## Kalman filter equations

The Kalman filter equations for the above system are:

$$\text{Measurement} \quad \begin{cases} \hat{x}_{t|t} = \hat{x}_{t|t-1} + \Sigma_{t|t-1} C^\top (C\Sigma_{t|t-1} C^\top + R)^{-1} (y_t - C\hat{x}_{t|t-1}) \\ \Sigma_{t|t} = \Sigma_{t|t-1} - \Sigma_{t|t-1} C^\top (C\Sigma_{t|t-1} C^\top + R)^{-1} C\Sigma_{t|t-1} \end{cases} \quad (2.44)$$

$$\text{Time update} \quad \begin{cases} \hat{x}_{t+1|t} = A_t \hat{x}_{t|t} \\ \Sigma_{t+1|t} = A_t \Sigma_{t|t} A_t^\top + Q \end{cases} \quad (2.45)$$

$$\text{Initial conditions} \quad \begin{cases} \hat{x}_{0|-1} = \tilde{x}_0 \\ \Sigma_{0|-1} = P_0 \end{cases} \quad (2.46)$$

### Measurement Update (Correction Step):

The first equation represents the update of the state estimate  $\hat{x}_{t|t}$ . It is a corrected estimate based on the new measurement  $y_t$ . The term  $\hat{x}_{t|t-1}$  is the predicted state from the previous timestep, and  $C$  is the measurement matrix that relates the state to the measurement. The product  $C\Sigma_{t|t-1} C^\top + R$  is the predicted measurement covariance, and  $R$  is the measurement noise covariance matrix. The entire term  $(C\Sigma_{t|t-1} C^\top + R)^{-1} (y_t - C\hat{x}_{t|t-1})$  is the Kalman gain multiplied by the measurement residual (the difference between the actual measurement and the predicted measurement). The second equation updates the estimate covariance  $\Sigma_{t|t}$ , which measures the estimated accuracy of the state estimate. This step essentially adjusts the estimated covariance to account for the new measurement.

### Time Update (Prediction Step):

The third equation predicts the state  $\hat{x}_{t+1|t}$  at the next timestep, based on the current corrected state estimate  $\hat{x}_{t|t}$ . The matrix  $A_t$  is the state transition model which is applied to the current estimate. The fourth equation predicts the state covariance  $\Sigma_{t+1|t}$  for the next timestep. This prediction includes the process noise  $Q$ , which accounts for the uncertainty in the prediction model.

### Initial Conditions:

These two equations provide the initial state estimate  $\hat{x}_{0|-1}$  and initial estimate covariance  $\Sigma_{0|-1}$  before any measurements are made.  $\tilde{x}_0$  is the initial state estimate, and  $P_0$  is the initial estimate covariance. These conditions are necessary to start the recursive Kalman filter process.

#### 2.4.4 PD control

In order to utilise altitude control on the quadcopter we have used a PD (Proportional-Derivative) controller. A PD controller is a control loop feedback mechanism which is widely used in industrial control systems. It is a type of linear feedback control system that combines two kinds of control:

- **Proportional control (P):** This part of the algorithm reacts to the current error, which is the difference between the set point and the processes current value. The proportional term analyses the error and produces a linear output based on the error. This results in the rapid response of the system to deviations from the desired setpoint, helping to stabilize the system by moving the process variable in the right direction. The Proportional gain is a variable parameter that sets the level of aggression of the PID controller in its response to error. A high  $K_p$  means a larger output for a given error – and,

therefore, a faster response of the system to make up for the error – but setting  $K_p$  too high will lead to instability in the form of gross oscillations about the setpoint.

- **Derivative (D):** The derivative term in a PD controller plays a crucial role in forecasting the system's future dynamics based on the current rate at which the error is changing. It acts as a form of predictive control, providing a damping force that enhances the stability of the system. By tempering the response generated by the proportional component, the derivative action effectively mitigates overshoot—preventing the system output from exceeding the desired setpoint. Increasing the derivative time ( $K_d$ ) parameter will cause the control system to react strongly to changes in the error term and will increase the speed of the overall control system response. Moreover, it contributes to a faster response by reducing the settling time, which is the time it takes for the system to stabilize within a certain range of the setpoint.

The general equation for a PD controller, given an error signal  $e[k]$  (the difference between the desired set-point and the actual process variable), can be expressed as:

$$u[k] = K_p e[k] + K_d \frac{e[k] - e[k-1]}{T_s} \quad (2.47)$$

where:

- $u[k]$  is the control output  $u$  at the  $k$ -th time step.
- $K_p$  is the proportional gain, a tuning parameter that scales the magnitude of the proportional term.
- $e[k]$  is the error between the set-point and the process variable at the  $k$ -th time step.
- $K_d$  is the derivative gain, a tuning parameter that scales the magnitude of the derivative term.
- $e[k] - e[k-1]$  is the difference between the error at the current time step and the error at the previous time step.
- $T_s$  is the sampling period or the time interval between successive measurements.

## Implementation

In order to calculate the altitude error ( $e$ ) the difference between the estimated altitude ( $z_{est}$ ) taken from the Kalman Filter shown above (2.4.3) and the altitude reference ( $z_{ref}$ ). The altitude reference's initial value is set at the altitude at which the quadcopter is situated at when the switch (c) is pressed on the radio, it can then be changed by changing the toggle (VRE) to increase or decrease the reference altitude, for more information on the switches please see Section:3.1.

$$e = z_{est} - z_{ref} \quad (2.48)$$

The control action ( $u$ ) is the sum of three terms: the equilibrium throttle setting ( $\tau_{eq}$ ), the proportional term, and the derivative term. The proportional term is the product of the proportional gain ( $K_p$ ) and the altitude error. The derivative term is the product of the derivative gain ( $K_d$ ) and the estimated vertical speed ( $v_{z_{est}}$ ).

$$u = \tau_{eq} + K_p e + K_d v_{z_{est}} \quad (2.49)$$

- $\tau_{eq}$  is the equilibrium throttle setting, a constant value to maintain hover.
- $K_p \cdot e$  is the proportional component, which scales the altitude error by the proportional gain.
- $K_d \cdot v_{z_{est}}$  is the derivative component, which scales the estimated vertical speed by the derivative gain.

In this implementation the tuning parameters were:

- Proportional Gain is set to 5
- Derivative Gain is set to 3
- Equilibrium Throttle is set to 0.4

#### 2.4.5 Altitude control system overview

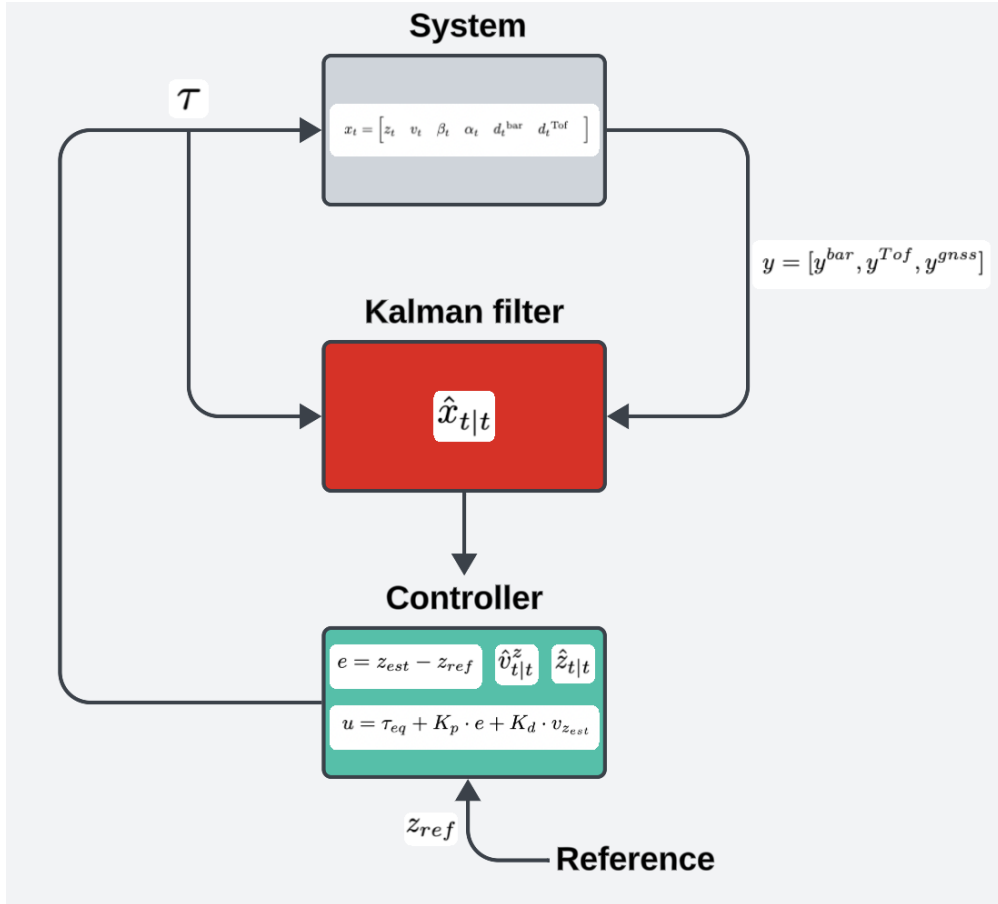


Figure 2.15: Altitude control system flowchart

As seen in the flowchart above in Figure:2.15 the system starts by defining the state estimate ( $x_t$ ) which then defines the output ( $y = [y^{\text{bar}}, y^{\text{Tof}}, y^{\text{gnss}}]$ ). The Kalman filter then uses the measurements  $y$  to update updates the state estimate ( $\hat{x}_{t|t}$ ) where the controller uses the updated altitude ( $\hat{z}_{t|t}$ ) to determine the error ( $e$ ) by subtracting the correct estimated altitude ( $z_{\text{est}}$ ) from the imputed reference altitude( $z_{\text{ref}}$ ). The PD controller then takes the pre defined throttle equilibrium ( $\tau_{eq}$ ) and updated estimated vertical velocity ( $\hat{v}_{t|t}^z$ ), computes a new throttle command  $u$  to adjust the altitude of the quadcopter.

## 2.4.6 Simulations

In the world of autonomous systems, behaviour prediction and control accuracy is critical, especially for systems with complicated dynamics like quadcopters. At the heart of this endeavour are simulations, which provide a flexible and perceptive environment for algorithm creation and validation. This section explores the extensive simulation environment that was meticulously developed to evaluate and improve the two essential parts of our control system: the proportional-derivative (PD) controller and the Kalman filter.

Across all simulations, Proportional Gain, Derivative Gain and Equilibrium Throttle are all set to the values denoted above, Section:2.4.4

The process noise covariance matrix  $Q$  is given by:

$$Q = \begin{bmatrix} 0.001^2 & 0 & 0 & 0 & 0 & 0 \\ 0 & 0.01^2 & 0 & 0 & 0 & 0 \\ 0 & 0 & (0.1(2.77 \times 10^{-6}))^2 & 0 & 0 & 0 \\ 0 & 0 & 0 & (0.1(1.74 \times 10^{-7}))^2 & 0 & 0 \\ 0 & 0 & 0 & 0 & 0.50^2 & 0 \\ 0 & 0 & 0 & 0 & 0 & 0.10^2 \end{bmatrix} \quad (2.50)$$

Where,  $\sigma_z, \sigma_v, \sigma_\alpha, \sigma_\beta$  are  $0.001, 0.01, 2.77 \times 10^{-6}$ , and  $1.74 \times 10^{-7}$ , respectively.

The measurement noise covariance matrix  $R$  is defined as:

$$R = \begin{bmatrix} (0.25(0.1))^2 & 0 & 0 \\ 0 & (0.075(0.1))^2 & 0 \\ 0 & 0 & (0.01(0.1))^2 \end{bmatrix} \quad (2.51)$$

Where,  $\sigma_{\text{bar}}, \sigma_{\text{gnss}}, \sigma_{\text{ToF}}$  are  $0.25 \times T_s, 0.075 \times T_s$ , and  $0.01 \times T_s$  respectively.

### Both $\alpha$ and $\beta$ are estimated

In the fist simulation  $\alpha$  and  $\beta$  along with the Time of Flight bias ( $d^{ToF}$ ), Barometer bias ( $d^{bar}$ ), altitude velocity and throttle reference are being predicted.

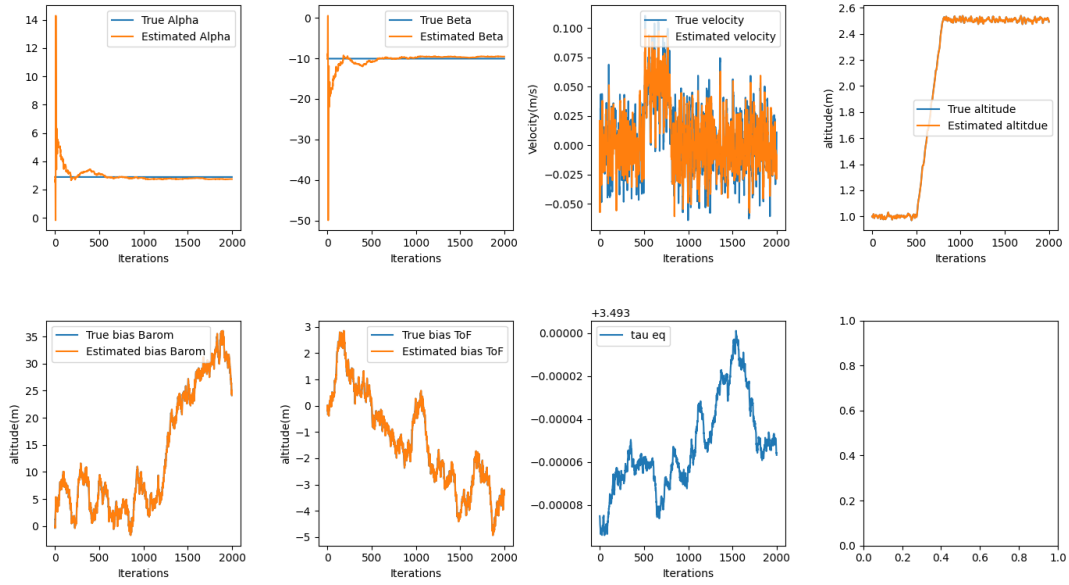


Figure 2.16: Simulation1: Both alpha and beta being predicted

In this simulation the quadcopters altitude control system's performance is evaluated. The system uses a Kalman filter for state estimation, tackling noise and sensor bias and a PD controller for altitude adjustments.

Observations from the simulation after processing 2000 time steps, with a sampling time  $T_s$  of 0.1 seconds, reveal several key dynamics;

The Kalman filter's ability to estimate values of  $\alpha$  and  $\beta$ , which relate throttle input to lifting as well as for ( $d^{ToF}$ ) and ( $d^{bar}$ ) in meters for the Time of flight and Barometer sensors respectively is clearly visible within this simulation. The estimated values for each do indeed converge in on the true values. This is a clear indication of the kalman filter's ability to conduct real-time estimation of the values even when system and measurement noise are present.

Beginning at a reference altitude of 0.5 meters, the quadcopters altitude begins to increase after the 500th time step to the 800th, due to the reference altitude being increased between these times. In response to this change the throttle reference ( $\tau$ ) is changed by the PD controller. The real and estimated altitudes suggest a controlled climb during this period, showing that the system has effectively guided the quadcopter to the new reference point using a PD controller.

The velocity graph showcases the control systems dynamic response to this change in altitude. As seen the velocity changes in-line with the altitude changes, this indicates that the PD controllers ability to change the quadcopters speed to achieve and sustain the target altitude has been well implemented.

The throttle reference graph denoted by  $\tau$  shows that the PD controller actively changes the throttle input in response to the new change in reference altitude. Once the altitude reference levels off after time-step 800 the throttle input begins to stabilise, indicating that the controller is reaching a new equilibrium point.

A well-tuned PD controller is shown by the system's minimum overshoot and smooth approach to the new altitude reference. The derivative component effectively dampens any oscillations, contributing to a swift yet stable climb to the desired altitude.

in conclusion, this simulation shows how the PD controller designed used in tandem with the Kalman filter may be used to successfully manage altitude in the quadcopter. The Controller adjusts the reference altitude and responds well to the changes posed on the quadcopter. The controller runs with precise state information thanks to the Kalman filter's skilful tracking and estimation of critical system parameters and sensor biases, making this a viable solution for altitude control in the real quadcopter.

#### **$\alpha$ is constant whilst $\beta$ is being estimated**

In the second simulation  $\alpha$  is set at as a constant and  $\beta$  is estimated along with the Time of Flight bias ( $d^{ToF}$ ), Barometer bias ( $d^{bar}$ ), altitude velocity and throttle reference are being predicted.

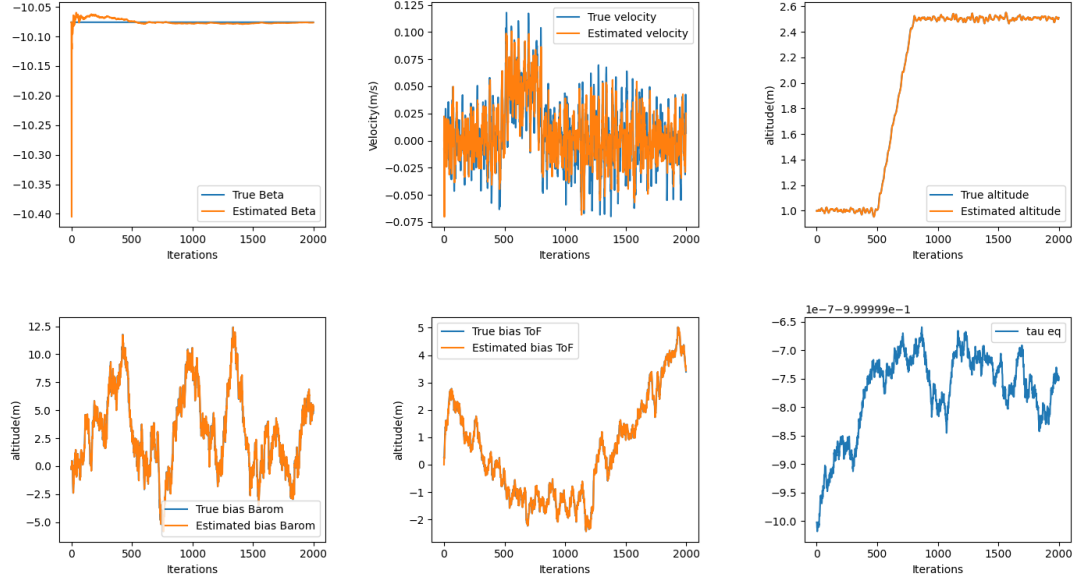


Figure 2.17: Simulation2: constant alpha and beta being predicted

In this simulation the quadcopters altitude control system's performance is evaluated. The system uses a Kalman filter for state estimation, tackling noise and sensor bias and a PD controller for altitude adjustments.

Observations from the simulation above Figure:2.17 after processing 2000 time steps, with a sampling time  $T_s$  of 0.1 seconds, reveal several key dynamics;

The kalman filter's ability to estimate values of  $\beta$ , as well as for  $d^{ToF}$  and  $d^{bar}$  in meters for the Time of flight and Barometer sensors respectively is clearly visible within this simulation, notably when compared to the simulation above (Figure:2.16)  $\alpha$  is no longer being estimated. The estimated values for each do indeed converge in on the true values. This is a clear indication of the kalman filter's ability to conduct real-time estimation of the values even when system and measurement noise are present.

Beginning at a reference altitude of 0.5 meters, the quadcopters altitude begins to increase after the 500th time step to the 800th, due to the reference altitude being increased between these times. In response to this change the throttle reference ( $\tau$ ) is changed by the PD controller. The real and estimated altitudes suggest a controlled climb during this period, showing that the system has effectively guided the quadcopter to the new reference point using a PD controller.

The velocity graph again showcases the control systems dynamic response to this change in altitude. As seen the velocity changes in-line with the altitude changes, this indicates that the PD controllers ability to change the quadcopters speed to achieve and sustain the target altitude has been well implemented.

The throttle reference graph denoted by  $\tau$  shows that the PD controller actively changes the throttle input in response to the new change in reference altitude. Once the altitude reference levels off after time-step 800 the throttle input begins to stabilise, indicating that the controller is reaching a new equilibrium point.

A well-tuned PD controller is shown by the system's minimum overshoot and smooth approach to the new altitude reference. The derivative component effectively dampens any oscillations, contributing to a swift yet stable climb to the desired altitude.

In conclusion, this simulation shows how the PD controller designed used in tandem with the Kalman filter may be used to successfully manage altitude in the quadcopter. While alpha is considered a constant in this scenario, not subject to estimation by the Kalman filter, the system's performance remains robust. The Controller adjusts the reference altitude and responds well to the changes posed on the quadcopter. The controller runs with precise state information thanks to the Kalman filter's skilful tracking and estimation of critical system parameters and sensor biases, making this a viable solution for altitude control in the real quadcopter.

#### **$\beta$ is constant whilst $\alpha$ is being estimated**

In the third simulation  $\beta$  is set at as a constant and  $\alpha$  is estimated along with the Time of Flight bias ( $d^{ToF}$ ), Barometer bias ( $d^{bar}$ ), altitude velocity and throttle reference are being predicted.

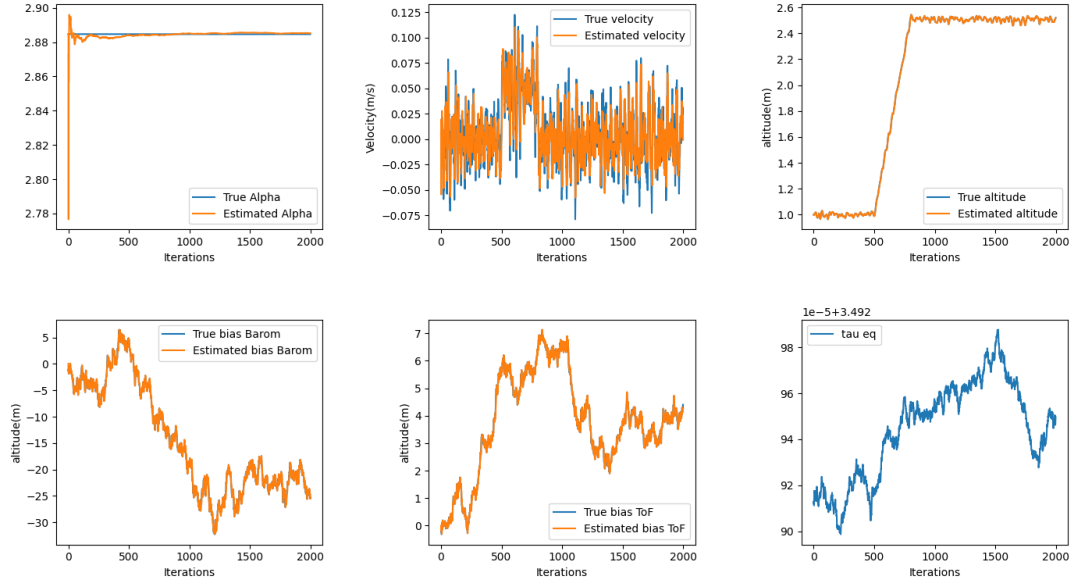


Figure 2.18: Simulation3: constant beta and alpha being predicted

In this simulation the quadcopters altitude control system's performance is evaluated. The system uses a Kalman filter for state estimation, tackling noise and sensor bias and a PD controller for altitude adjustments.

Observations from the simulation above Figure:2.18 after processing 2000 time steps, with a sampling time  $T_s$  of 0.1 seconds, reveal several key dynamics;

The kalman filter's ability to estimate values of  $\alpha$ , as well as for  $d^{ToF}$  and  $d^{bar}$  in meters for the Time of flight and Barometer sensors respectively is clearly visible within this simulation, notably when compared to the simulation above (Figure:2.16)  $\beta$  is no longer being estimated. The estimated values for each do indeed converge in on the true values. This is a clear indication of the kalman filter's ability to conduct real-time estimation of the values even when system and measurement noise are present.

Beginning at a reference altitude of 0.5 meters, the quadcopters altitude begins to increase after the 500th time step to the 800th, due to the reference altitude being increased between these times. In response to this change the throttle reference ( $\tau$ ) is changed by the PD controller. The real and estimated altitudes suggest a controlled climb during this period, showing that the system has effectively guided the quadcopter to the new reference point using a PD controller.

The velocity graph again showcases the control systems dynamic response to this change in altitude. As seen the velocity changes in-line with the altitude changes, this indicates that the PD controllers ability to change the quadcopters speed to achieve and sustain the target altitude has been well implemented.

The throttle reference graph denoted by  $\tau$  shows that the PD controller actively changes the throttle input in response to the new change in reference altitude. Once the altitude reference levels off after time-step 800 the throttle input begins to stabilise, indicating that the controller is reaching a new equilibrium point.

A well-tuned PD controller is shown by the system's minimum overshoot and smooth approach to the new altitude reference. The derivative component effectively dampens any oscillations, contributing to a swift yet stable climb to the desired altitude.

In conclusion, this simulation shows how the PD controller designed used in tandem with the Kalman filter may be used to successfully manage altitude in the quadcopter. While  $\beta$  is considered a constant in this scenario, not subject to estimation by the Kalman filter, the system's performance remains robust. The Controller adjusts the reference altitude and responds well to the changes posed on the quadcopter. The controller runs with precise state information thanks to the Kalman filter's skilful tracking and estimation of critical system parameters and sensor biases, making this a viable solution for altitude control in the real quadcopter.

## Simulations conclusion

In conclusion, the simulation where both  $\alpha$  and  $\beta$  were being estimated shown in Figure:2.16 has shown notable effectiveness. The Kalman filters ability to estimate values in real time, allowing them to converge quickly on there real values should not go un noted. The accurate estimation of the Kalman filter forms the basis for the Proportional Derivative (PD) controllers ensuring its responses are reliable on data.

The Kalman filters efficiency is evident in this simulation, despite requiring estimation for both  $\alpha$  and  $\beta$  the system still displays a good degree of stability and control. The PD controller allows the system to respond to a changing reference altitude without any oscillations. This suggests that the inclusion of  $\alpha$  and  $\beta$  has not negatively impacted the systems performance when coparing the results from the other two simulations in figures:2.17 and 2.18.

The results show that the decision to estimate both alpha and beta within the Kalman filter formulation for sensor fusion of altitude sensors in the system, is promising. This system, when designed and implemented in the quadcopter using a PD controller, can not only maintain the altitude accurately but also respond

smoothly and seamlessly in the event of any changes in the reference altitude. It is the combination of all the elements of the system that make it a feasible option for real-life use. The entire proposition offers a high level of fine control that is not only ideal but also essential for autonomous quadcopter flight.

## 2.5 Position control (not yet implemented)

The incorporation of an advanced position control system is critical for optimising the quadcopter's performance and stability, especially in dynamic conditions. This system makes use of the accuracy and dependability of the onboard GNSS module and works in conjunction with the altitude control mechanism described in Section:2.4.3. The GNSS module provides essential latitude and longitude data that establishes the groundwork for real-time position control.

When the system is activated by, toggling switch C to its range-2 position as described in Section:3.2, it instantly locks in the altitude and current coordinates as the reference points. This critical point initiates highly responsive control loops in which these reference values serve as the basis for the navigation and stabilisation tasks that follow.

With these reference points in mind, the control system uses a Proportional-Derivative (PD) controller, which is explained in detail in Section:2.4.4, to carefully control altitude. By doing this, the quadcopter is guaranteed to keep a constant elevation, which is essential for efficient position control. In addition, the quadcopter's movement is controlled across all axes not just the z-axis by incorporating a Proportional-Integral-Derivative (PID) controller, which is covered in more detail in Section:2.5.3. A harmonious balance between location precision and altitude stability is ensured by this dual-controller approach.

The quadcopter should hover with high accuracy because of the smooth integration of various control mechanisms. The system can instantly make modifications by continuously comparing the current positioning data with the predefined reference points. This degree of responsiveness is essential for adjusting to outside factors like wind currents and making sure the quadcopter's position is unaffected by them.

Furthermore, new applications where accuracy and stability are critical, such as autonomous navigation, search and rescue, aerial photography, are made possible by this sophisticated position control system.

### 2.5.1 Global positioning to Local positioning

In order for the system to be able to read the reference points accurately, conversion from global position to local position will be needed.

Global positioning refers to its location on a given coordinate system such as GNSS module latitude and longitude. These values are useful when attempting to find the Quadcopters position on a global scale. For our use a better approach is having a local position relative to a given standpoint or start point.

By utilising the base station in Section:3.14 coordinates of the rover module can be parsed relative to the base station in a local frame along a 2D plane.

First the quadcopters Global coordinates (latitude,longitude and altitude) are converted to the ECEF coordinate system. This system represents points with Cartesian coordinates (x, y, z) with the origin at the center of the Earth.

Next the ECEF coordinates will be translated into a north, east down system, using a rotation matrix that accounts for the orientation of the Earth's surface at the base station relative to the rover module.

Below, you can view graphs that depict the rotational differences along an axis between local and global positioning systems.

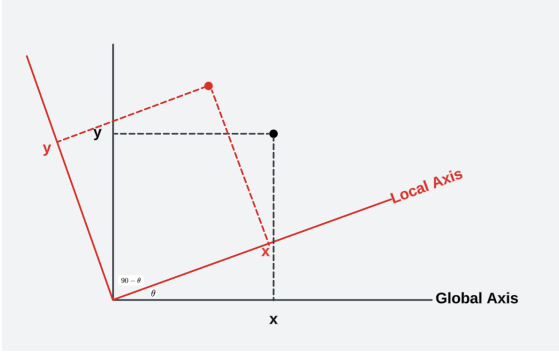


Figure 2.19: Graph representing the difference between global and local positioning

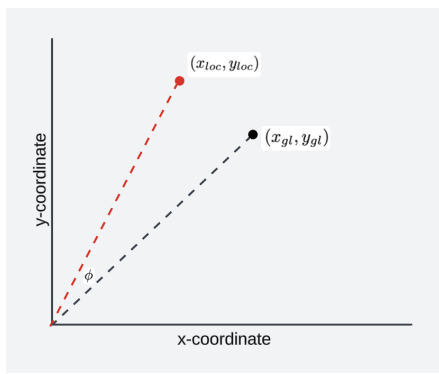


Figure 2.20: Global vs Local position

In order to find the local x and y coordinates denoted by  $x_{loc}, y_{loc}$  in Figure 2.20 a rotation matrix is used in the following equation.

$$\begin{bmatrix} x_{loc} \\ y_{loc} \end{bmatrix} = \begin{bmatrix} \cos\phi & -\sin\phi \\ \sin\phi & \cos\phi \end{bmatrix} \begin{bmatrix} x_{gl} \\ y_{gl} \end{bmatrix} \quad (2.52)$$

where,  $\phi$  represents the heading taken from the compass in the IMU

## 2.5.2 Modelling

The model used for Position control can be defined as,

- **Position Update:**

$$p_{t+1} = p_t + T \cdot v_t$$

- **Velocity Update:**

$$v_{t+1} = v_t + T \left( R(\theta_t^r, \theta_t^p) \begin{bmatrix} 0 \\ 0 \\ \dot{z}_t \end{bmatrix} + \begin{bmatrix} 0 \\ 0 \\ -g \end{bmatrix} - \begin{bmatrix} A^x & 0 & 0 \\ 0 & A^y & 0 \\ 0 & 0 & A^z \end{bmatrix} v_t \right)$$

- **Attitude Update for Roll and Pitch:**

$$\theta_{t+1}^r = \theta_t^r + \frac{T}{\omega^r} (K^r \theta_t^{r,ref} - \theta_t^r)$$

$$\theta_{t+1}^p = \theta_t^p + \frac{T}{\omega^p} (K^p \theta_t^{p,ref} - \theta_t^p)$$

where  $p_t = (p_t^x, p_t^y, p_t^z)$  and  $v_t$  are the position and velocity of the quadcopter in the global frame of reference.  $\theta^p$  and  $\theta^r$  are the pitch and roll angles.  $\theta^{p,ref}$  and  $\theta^{r,ref}$  are the pitch and roll references that are sent to the controller.  $\dot{z}_t$  is the vertical acceleration in the z-axis as defined in 2.4.3, while  $A^x, A^y, A^z$  are the linear drag coefficients.  $T$  is the sampling time.

The attitude control system is then modelled, time constants  $\omega^p$  and  $\omega^r$  and gains  $K^r$  and  $K^p$  for the roll and pitch.

Finally  $R(\theta^r, \theta^p)$  can be defined as euler angles in rotation matrix form as

$$R(\theta^r, \theta^p) = R^y(\theta^p)R^x(\theta^r) \quad (2.53)$$

where,

$$R^x(\theta^r) = \begin{bmatrix} 1 & 0 & 0 \\ 0 & \cos(\theta^r) & -\sin(\theta^r) \\ 0 & \sin(\theta^r) & \cos(\theta^r) \end{bmatrix}, \quad (2.54)$$

$$R^y(\theta^p) = \begin{bmatrix} \cos(\theta^p) & 0 & \sin(\theta^p) \\ 0 & 1 & 0 \\ -\sin(\theta^p) & 0 & \cos(\theta^p) \end{bmatrix} \quad (2.55)$$

These equations were derived and changed from [16]

### 2.5.3 PID control

In order to utilise position control on the quadcopter PID (Proportional-integral-Derivative) controller's have been used, one for latitude ( $y_g l$ ) control and the other for longitude ( $x_g l$ ) control. A PID controller is a control loop feedback mechanism which is widely used in industrial control systems. It is a type of linear feedback control system that combines three kinds of control:

- **Proportional control(P):** This part of the algorithm reacts to the current error, which is the difference between the set point and the processes current value. The proportional term analyses the error and produces a linear output based on the error. This results in the rapid response of the system to deviations from the desired setpoint, helping to stabilize the system by moving the process variable in the right direction. The Proportional gain is a variable parameter that sets the level of aggression of the PID controller in its response to error. A high Kp will mean a larger output for a given error – and, therefore, a faster response of the system to make up for the error – but setting Kp too high will lead to instability in the form of gross oscillations about the setpoint.
- **Integral (I):** The integral control deals with the accumulated error over time by emphasising the difference between the system's actual performance and the planned reference setpoint. The integral term adds up previous errors, supplying a corrective force proportionate to the length and size of the deviation, in contrast to the proportional component, which just reacts to the current error. This feature of the controller ensures that the process variable finally converges to the setpoint and is especially useful at removing steady-state faults. The controller's sensitivity to the cumulative mistake is controlled by the Integral gain, or Ki. A well adjusted Ki can minimise offset considerably, but an overly high value could cause oscillations and overshooting, which would compromise the stability of the system.
- **Derivative(D):** The derivative term in a PD controller plays a crucial role in forecasting the system's future dynamics based on the current rate at which the error is changing. It acts as a form of predictive control, providing a damping force that enhances the stability of the system. By tempering the response generated by the proportional component, the derivative action effectively mitigates overshoot—preventing the system output from exceeding the desired setpoint. Increasing the derivative time (Kd) parameter will cause the control system to react strongly to changes in the error term and

will increase the speed of the overall control system response. Moreover, it contributes to a faster response by reducing the settling time, which is the time it takes for the system to stabilize within a certain range of the setpoint.

generally a PID controller is given by the following equation:

$$u(t) = K_p e(t) + K_i \int_0^t e(\tau) d\tau + K_d \frac{d}{dt} e(t) \quad (2.56)$$

where:

- $u(t)$  is the controller output at time  $t$ .
- $e(t)$  is the error between the setpoint and the process variable at time  $t$ .
- $K_p$  is the proportional gain, a tuning parameter that scales the magnitude of the proportional term.
- $K_i$  is the Integral gain, a tuning parameter that determines the reaction based on the sum of recent errors, providing a correction based on the historical cumulative error, which helps eliminate steady-state error.
- $K_d$  is the derivative gain, a tuning parameter that scales the magnitude of the derivative term.
- $\int_0^t e(\tau) d\tau$  represents the Integral of the error over time from 0 to the current time  $t$ , accounting for the accumulation of past errors.
- $\frac{d}{dt} e(t)$  is the rate of change of the error (derivative of the error with respect to time)

## Implementation

In order to implement Position control in the quadcopter two PID controllers need to be utilised, one for control of the latitude data and the other for longitude data.

In order to calculate the position error ( $e$ ) the difference between the current position and the reference position must be calculated. For both latitude, longitude and altitude controllers the equations would look like this, where  $x$  represents longitude,  $y$  represents latitude and  $z$  is the altitude in local format(Section:2.5.1):

$$e_x = x_{\text{current}} - x_{\text{ref}} \quad (2.57)$$

$$e_y = y_{\text{current}} - y_{\text{ref}} \quad (2.58)$$

$$e_z = z_{\text{current}} - z_{\text{ref}} \quad (2.59)$$

The control action ( $u$ ) is the sum of three terms: the baseline control inputs( $u_{\text{baseline}}$ ), the proportional term, the integral term and the derivative term. The proportional term is the product of the proportional gain ( $K_p$ ) and the altitude error. The integral term is the product of the integral gain( $K_i$ ) and the position errors over time. The derivative term is the product of the derivative gain ( $K_d$ ) and the rate of change in error.

The continuous-time pitch control equation, where  $\theta^p$  represents the pitch angle and  $v_x$  is the velocity along the  $x$  axis, is given by:

$$\theta_t^{p,\text{ref}} = K_{p,x} \cdot e_x + K_{i,x} \cdot \sum e_x \Delta t + K_{d,x} \cdot v_x \quad (2.60)$$

Similarly, the roll control equation, where  $\theta^r$  represents the roll angle and  $v_y$  is the velocity along the  $y$  axis, is given by:

$$\theta_t^{r,\text{ref}} = K_{p,y} \cdot e_y + K_{i,y} \sum e_y \Delta t + K_{d,y} \cdot v_y \quad (2.61)$$

The altitude control equation, where  $z$  represents the altitude and  $v$  is the velocity along the  $z$  axis, is given by

$$u_z = \tau_{eq} + K_{p,z} \cdot e_z + K_{i,z} \sum e_z \Delta t + K_{d,z} \cdot v_z \quad (2.62)$$

where  $\theta_p/\theta_r$  represents the reference angle that we want to achieve.  $\sum e_y \Delta t$  is the integral of the error over time, which helps in eliminating steady-state errors.  $v_x/v_y/v_z$  is the velocity along the specified axis, used for derivative control to anticipate changes in the system.

#### 2.5.4 Position control system overview

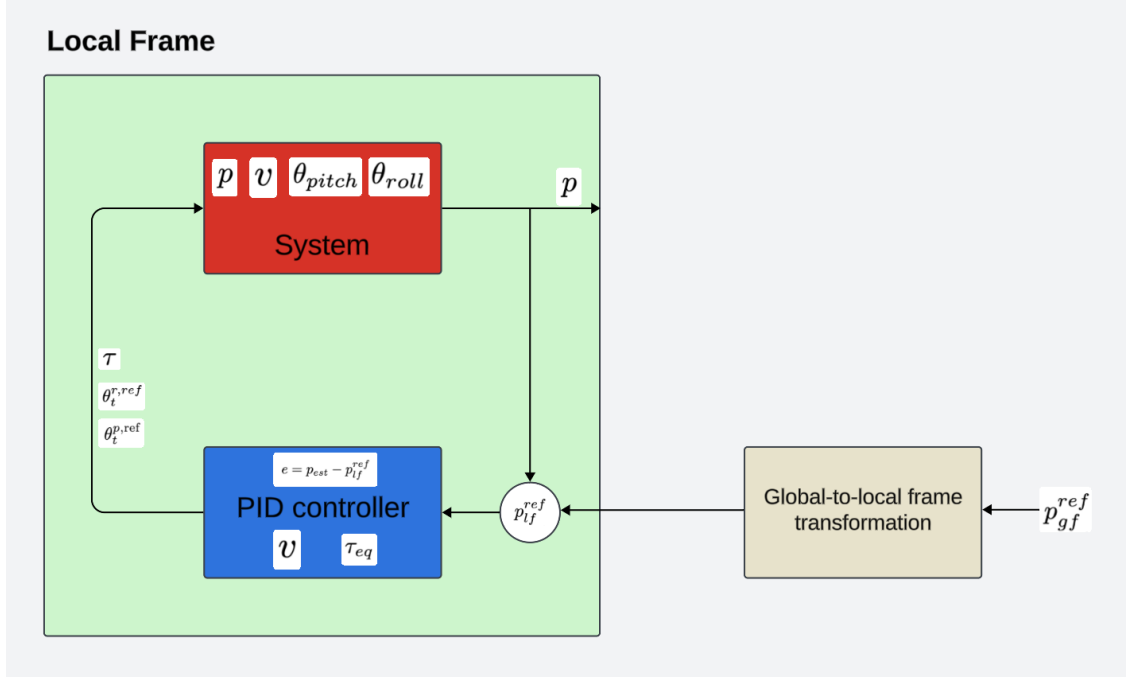


Figure 2.21: Position control system overview

The flowchart illustrates the position control system within a local frame of reference, the System processes the state variables; the position vector ( $p$ ), the velocity vector ( $v$ ), and the orientation angles for pitch ( $\theta_{\text{pitch}}$ ) and roll ( $\theta_{\text{roll}}$ ). The system's output is the current position vector ( $p$ ), which serves as an input to the subsequent PID Controller.

The PID controller receives this position vector ( $p$ ) and compares it to a local reference position vector ( $p_{\text{if}}^{\text{ref}}$ ), calculating the error ( $e$ ). This error, along with the vehicle's current velocity ( $v$ ) and a predefined equilibrium thrust ( $T_{\text{eq}}$ ), are used to determine the necessary control signals. The reference pitch ( $\theta_{t,\text{ref}}^{\text{pitch}}$ ) and roll ( $\theta_{t,\text{ref}}^{\text{roll}}$ ) angles are utilised to generate the control signals to correct the vehicle's orientation and maintain its position as well as the updated throttle signal( $\tau$ ).

The *Global-to-local frame transformation* module, takes a reference position in the global frame ( $p_{\text{gf}}^{\text{ref}}$ ) and converts it to a corresponding local frame reference position ( $p_{\text{lf}}^{\text{ref}}$ ).

The PID controller, which modifies the vehicle's pitch and roll depending on the transformed reference position, the interaction between these system steps guarantees that the vehicle retains the intended position within the local frame. For the navigation control module in a three-dimensional environment to function accurately and timely, this control loop is indispensable.

### 2.5.5 Simulations

The accuracy of control mechanisms is critical in the field of autonomous systems, especially for robots and quadcopters that have to manoeuvre through challenging settings. The use of simulations, which provide a flexible and insightful platform for designing and testing algorithms, is essential to improving these control systems. The purpose of this simulation environment is to evaluate and improve Position Control with Proportional-Integral-Derivative controllers. By modifying control inputs in response to variations between the desired and present positions, PID controllers play a crucial role in autonomous systems' capacity to achieve desired position and stability. By using complex simulations, we are able to precisely adjust the PID parameters to maximise system performance in a variety of scenarios, guaranteeing accuracy and resilience in the control of self-governing systems.

Thought the simulations below the PID gains we set are as follows:

- $K_p$ : 2.0
- $K_i$ : 0.2
- $K_d$ : 0.05

## Quadcopter manouvering to one waypoint/target point

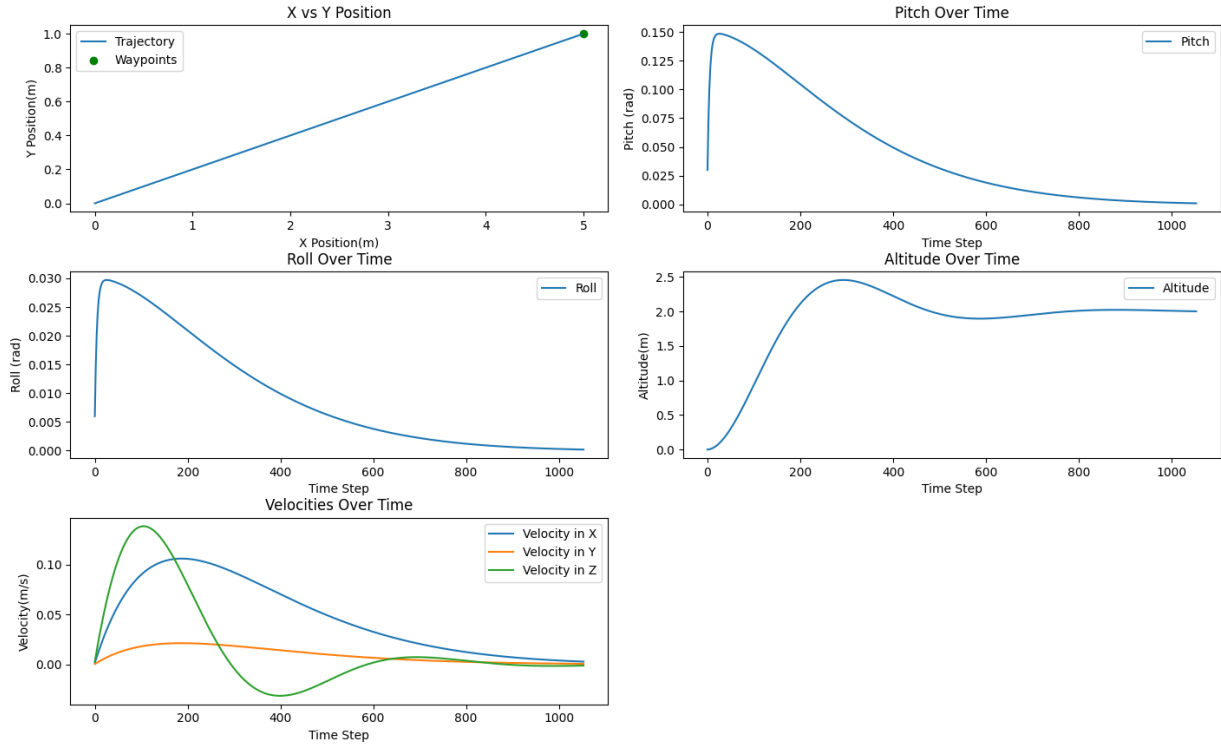


Figure 2.22: Path of quadcopter from Initial to reference position

The quadcopter's navigation capability is analysed during this advanced simulation. The quadcopter's ability to actively correct its course is made possible by Proportional-Integral-Derivative (PID) controllers (one for pitch control, one for roll control and one for altitude control).

The x, y and z velocities demonstrate variations in the velocity chart at the beginning showing a initial strong reaction in both x and z and velocities as a result of the PID controllers reaction to their larger position error when comparing the current to the refferance position. On the other hand the y velocity doesnt move as fast as its displacement from its target coordinate is not as big. Finally, all velocitys converge on 0 as the quadcopter has reached its desired point.

The quadcopter navigation system is also faced with a difficult dynamic situation, brought about by its target positions location. Both pitch, roll and altitude PID controllers are used simultaneously in this simulation.

We can see that both pitch and roll angles are making adjustments in order for the quadcopter to reach its desired target position. It is notable that the roll angle is less than the Pich as it has less distance to travel on the y axis.

Finally, the dones altitude can be seen converging on its target altitude of 2m with a slight overshoot.

In conclusion, the quadcopter PID control systems works well, In was able to reach its desired position with minimal overshoot.This degree of control, which is significant for a number of real-world applications, validates the system's efficacy and dependability and represents a promising standard for durable quadcopter navigation systems.

## Quadcopter manouvering around different waypoints

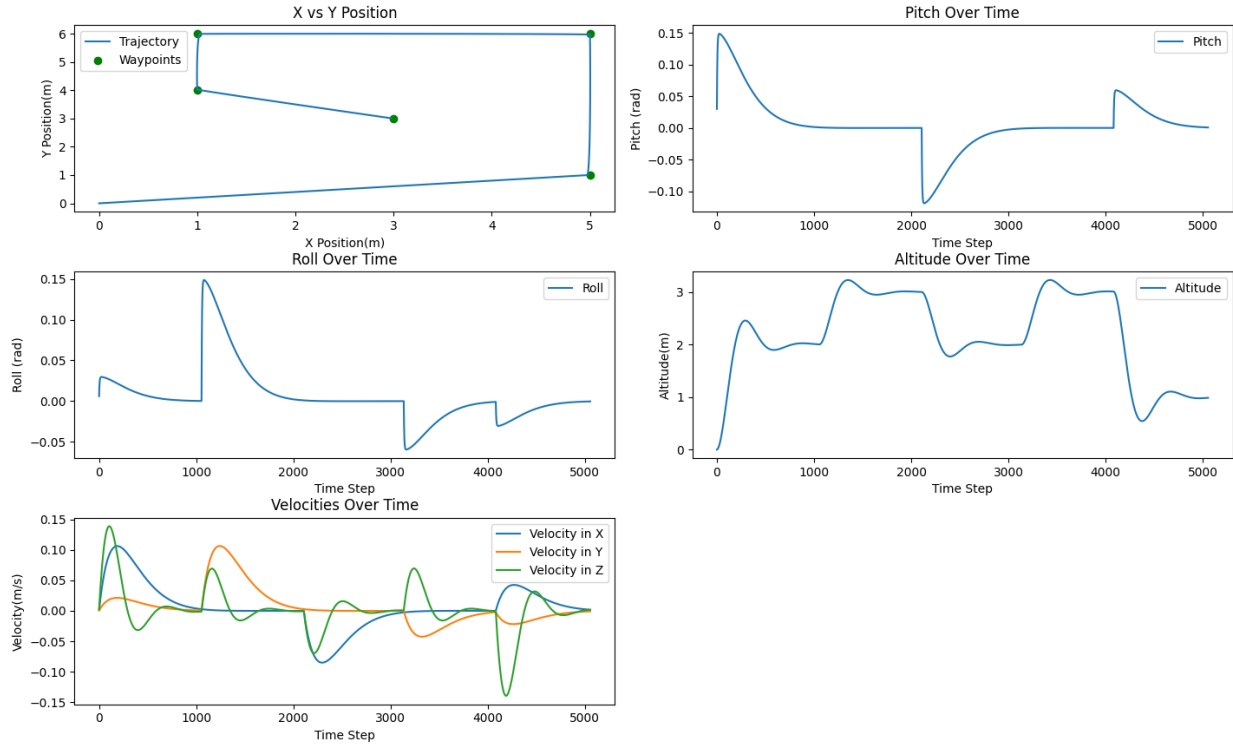


Figure 2.23: Path of quadcopter from Initial position around waypoints

The quadcopter's navigation capability is analysed during this advanced simulation as it manoeuvres between various different per determined way points. when the quadcopter comes within 3cm from said waypoint it is changed to the next one, and so on.

The quadcopter's ability to actively correct its course is made possible by Proportional-Integral-Derivative (PID) controllers (one for pitch control, one for roll control and one for altitude) with little to no overshoot when flying between waypoints. The flight course instinctively reacts to changes in waypoints, by adjusting its pitch and roll angles as well as its altitude to travel to the next one. The velocities on the x, y and z axis are ever changing and consistently converging on the desired position.

The quadcopter navigation system is also faced with a difficult dynamic situation, brought about by its everchanging waypoints. Both pitch, roll and altitude PID controllers are used simultaneously in this simulation.

Finally, the quadcopter PID control systems works well as it moves between waypoints; the results of the simulation exercise indicate high flexibility, accurate results, and stability proving the controllers effectiveness. There is little to no overshoot on when flying between waypoints and all angles and velocities converge on the waypoints.

# Chapter 3

## hardware

This section outlines the various hardware that is used in forming the overall structure of the quadcopter.

### 3.1 Motors



Figure 3.1: 1400KV Brushless Motor

The PROPDRAIVE v2 3536 1400KV Brushless Outrunner Motor is designed to offer solid performance right out of the box. It features tight windings, smooth bearings, precision cut stator, and balanced rotors for reliable operation.

Key specifications include its 1400KV (Kilo Volt) rating, meaning that for every 1 Volt applied the motor will turn 1400 times. A maximum current of 45A, and compatibility with the Skywalker 50A ESC's which we are using below (Section:3.6). The motor is suitable for use with 3-4 cell batteries, again making it compatible with the 5500mAh 4S 70C LiPo Battery's being used (Section:3.9). It has 25mm bolt holes with an M3 bolt thread. It weighs around 121g and comes with 3.5mm bullet connectors.

## 3.2 Radio



Figure 3.2: Radio Controller with Pitch, Roll, Yaw, and Throttle Indicators

## 3.3 Receiver



Figure 3.3: Radiolink R12DS 2.4GHz RC Receiver

The radio transmitter and receiver pairs used for this project are the RadioLink AT10II (Tx) and R12DS (Rx), which are depicted in Figures 3.2 and 3.3, respectively. At 2.45GHz bandwidth, the transmitter can deliver data across 12 channels. Table:3.1 presents the channel mapping for the 12 channels.

The SBUS communication protocol is supported by the RadioLink R12DS receiver. In order to read the data from the 12 radio channels, the receiver is connected to the Raspberry Pi via SBUS with the aid of the connector. The Raspberry Pi reads the radio data as a bit-array, and Table:3.1 displays the decoded data channel and ranges.

The physical control sticks, switches, and knobs of the transmitter are represented as data elements in Table 3.1's column Mapping. The column labelled 'Channel number' has their matching channel number.

Channel number/ data index	Mapping	Signal range	Mapped range	Purpose
0	Yaw rate	{300, 1700}ms	[-3000, 3000]°/s	Yaw rate reference
1	Pitch	{300, 1700}ms	[-30, 30]°	Pitch reference
2	Throttle	{300, 1700}ms	[0, 900]ms	Throttle reference
3	Roll	{300, 1700}ms	[-30, 30]°	Roll reference
4	Switch C	{300,1000,1700}ms	{0, 1, 2}	Manual, Altitude Hold, Position control
5	VRA	{300, 1700}ms	[0, 1]%	P Gain (Quaternion Gain)
6	VRC	{300, 1700}ms	[0, 1]%	D Gain (Angular Velocity Gain)
7	VRB	{300, 1700}ms	[0, 1]%	(Yaw Angular Velocity Gain)
8	Switch B	{300, 1700}ms	{False, True}	Arm
9	Switch A	{300, 1700}ms	{False, True}	Save log
10	Switch D	{300, 1700}ms	{False, True}	Kill
11	VRE	{300, 1700}ms	[-0.25, 0.25]m	Change Altitude Reference

Table 3.1: RC Controller Channel Mapping

The data is sent by the transmitter in ascending order according to the channel number; that is, the data packet begins with channel 0 and concludes with channel 11 data.

The receiver reads the data channels beginning with channel 0 and ending with channel 11. The term 'raw data' is now used to describe this received data. The column labelled 'Signal range' displays the actual range of the raw data that was received; the units used are milliseconds. The Raspberry Pi uses SBUS to read this raw data.

The Raspberry Pi then processes and remaps the raw data to fit the control algorithm with the aid of a computer programme. The remapped ranges are displayed in the column Mapped range, and the remapped purpose is displayed in the Purpose column. The generated references for the attitude controller are the roll reference, throttle reference, pitch reference, and yaw rate reference in the Purpose column. To provide the controller commands room, the throttle reference is set to its maximum at 900 ms.

The ESP32 receives the state of Switch B and Switch D as well as the attitude reference data. The ESP32 arms and kills the quadcopter in accordance with the data from switches B and D. The attitude reference is used by the ESP32's attitude controller algorithm to determine what control actions are required. In Chapter 2.4.3, the attitude dynamic principles is covered.

The Raspberry Pi is instructed to save the flight data logs into a Comma-separated values (CSV) file by means of switch A. Turning switch A on and off many times will save multiple flight logs in a single flight. It is advised to land the quadcopter first before storing flight logs.

The switch C is a three-way switch with three states (0, 1, 2), and Manual, Altitude Hold, position hold are the mappings for each state. The throttle signal from the transmitter is sent to the attitude controller while switch C is in the manual mode and Position hold. Switch C's altitude hold mode activates the Raspberry Pi's altitude controller and altitude Kalman filter algorithms, which in turn override the transmitter's throttle reference command. The current altitude reference is adjusted by  $\pm 0.25$  metres in altitude hold mode using gain 4. In the position control mode the reference latitude and longitude are sent to the Raspberry Pi's altitude controller where the PID controller aims to keep the Quadcopter in the same position.

The trimmers can be used to tune the gains of the control algorithms. When tuning the attitude controller channel numbers 5, 6, 7 are set to Quaternion Gain, Angular Velocity Gain and Yaw Angular Velocity Gain respectively (as denoted by brackets in table:3.1). By default the trimmers are set to tune the altitude

controller with channel numbers 5 and 6 tuning the P Gain and D Gain ie.  $K_p$  and  $K_d$  (see Equation 2.49) respectively. Furthermore, channel 11 is used to Change Altitude Reference when in altitude control mode at a max rate of 4 cm/s.

## 3.4 Flight Controller

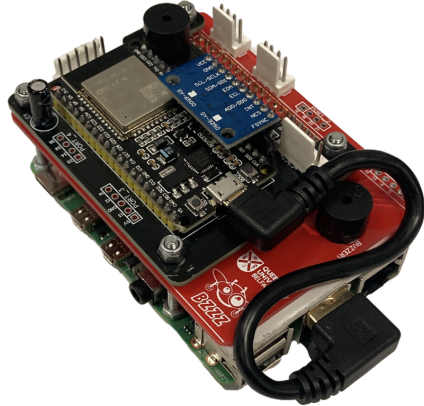


Figure 3.4: Flight controller

The flight controller is made up of two main components:

- Raspberry Pi
- ESP32

### 3.4.1 Raspberry Pi



Figure 3.5: Raspberry Pi

The Raspberry Pi is a particularly good option for inclusion into a quadcopter project because of its powerful processing and multitasking properties. With a potent quad core Cortex-A72 (ARM v8) 64-bit SoC clocked at 1.5GHz, the Broadcom BCM2711, the Pi 4B is well-suited to manage intricate calculations and numerous code executions concurrently. This is critical for a quadcopter, as it handles multiple tasks at once, including processing real-time sensor data and flying control algorithms. It is also the perfect brain for a quadcopter because of its small size, low power consumption, and plenty of GPIO pins for peripheral connections. This combination enables an aerial platform that is lightweight, adaptable, and extremely customisable.

The Raspberry Pi can run advanced computer vision and control algorithms utilising Python programming language because of its greater clock speed of 1.5GHz. This is essential for implementing algorithms for position and altitude control in a fully autonomous quadcopter. Because these algorithms only need to operate at a few hertz (5 to 10 Hz), the Raspberry Pi is an appropriate candidate. Pi is linked to a radio receiver module, which collects reference data from the radio controller.

The Raspberry Pi is implemented with the algorithms for position control, altitude hold, and manual mode. The Pi transfers the reference data to the ESP's attitude control algorithm in the manual mode, allowing for a completely manual flight. When in altitude hold mode, the Pi sends a modified throttle reference signal to the ESP in order to automatically track a reference altitude using an altitude hold control algorithm and a Kalman filter. When in position control mode, the Pi controls the quadcopter's horizontal position by sending the ESP adjusted latitude and longitude references. Refer to Chapter 2.4 for further information regarding the control algorithms.

### 3.4.2 ESP32



Figure 3.6: esp32

The ESP32 stands out as an exceptionally versatile and cost-effective microcontroller. This particular microcontroller stands out due, to its 32 bit architecture and the capability to run at a system clock speed of up to 240MHz with the version utilised in this project operating at 160MHz. This ensures processing power for handling demanding tasks.

A crucial aspect for a quadcopter is an attitude control system, which requires a microcontroller of performing pulse width modulation (PWM) at high frequencies preferably above 50Hz to ensure precise control over motor speeds. The ESP32s PWM capabilities along with its 160MHz clock speed make it a great choice for real time control operations. The strong community support and extensive documentation further enhance its suitability for projects offering developers an array of resources to utilise.

In the quadcopter project the ESP32 functions as the bridge between the Raspberry Pi and the quadcopters hardware such, as speed controllers (ESCs) and motors. It implements an attitude control algorithm written in python to maintain stability and respond to navigation commands. Using UART communication the ESP32 gets flight details from the Raspberry Pi, such, as orientations and throttle configurations. It then sends back flight information to ensure coordination of control systems for top notch flight efficiency. This interaction showcases the ESP32s ability to operate within a system of components proving its worth, in creating cutting edge aerial vehicles.

### 3.5 Inertial Measurement Unit (IMU)

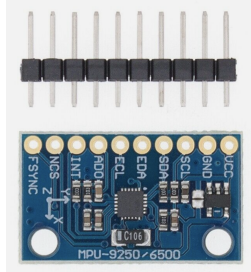


Figure 3.7: IMU

The MPU9250 integrates a 3-axis gyroscope, a 3-axis accelerometer, and a 3-axis magnetometer. This 9 DoF capability allows it to provide comprehensive data on the quadcopter's orientation, acceleration, and magnetic heading, enabling precise control and stabilization.

Its small footprint makes it ideal for use in compact devices like quadcopters, where space is at a premium and every gram of weight matters for flight efficiency and duration.

The MPU9250 is designed for low power consumption, which is crucial for battery-operated devices like quadcopters to maximize flight time.

It offers high-resolution sensor data, which is essential for maintaining stable flight and accurate navigation in a quadcopter. This precision enables the execution of complex manoeuvres and stability in various flying conditions. The gyroscope in the MPU9250 offers selectable full-scale ranges of  $\pm 250$ ,  $\pm 500$ ,  $\pm 1000$ , and  $\pm 2000$  degrees per second (dps). This allows for fine-tuning the sensitivity based on the specific requirements of the quadcopter, enabling precise measurement of rotational motion. The accelerometer provides selectable full-scale ranges of  $\pm 2g$ ,  $\pm 4g$ ,  $\pm 8g$ , and  $\pm 16g$ . This adaptability allows the device to accurately measure acceleration due to gravity and motion, contributing to effective motion tracking and stabilization. The magnetometer offers a full-scale range of  $\pm 4800 \mu T$ , allowing for precise measurements of the Earth's magnetic field. This sensitivity is key for accurate heading information, vital for navigation and maintaining a desired flight path.

The MPU9250's ability to output data from all nine sensors (gyroscope, accelerometer, magnetometer) allows for advanced sensor fusion algorithms, such as Kalman filtering, to provide highly accurate and reliable orientation and motion data.

For the above reasons as well as its low cost the MPU9250 IMU has been chosen.

This project utilises both I2C and SPI protocols for communication, with the MPU9250 IMU connected to the ESP 32 WROOM using the I2C protocol at a data transmission rate of 400KHz. Through the I2C protocol, the ESP 32 WROOM, serving as the master device on the bus, retrieves sensor data from the IMU, which functions as the slave device. The MPU9250 IMU offers various configurable measurement scales for its sensors, with the specific ranges employed in the quadcopter being: Gyroscope  $\pm 2000$  degrees per second (dps), accelerometer  $\pm 16g$  and Magnetometer  $\pm 4800\mu T$ .

### 3.6 ESC's (Electronic Speed Controller)



Figure 3.8: ESC (Electronic Speed Controller)

Designed specifically for quadcopters, the Skywalker 50A V2 is a brushless electronic speed controller (ESC). It can withstand peaks of up to 70A and runs at a constant 50A current, making it compatible with the motors above (Section:3.1). This ESC has an integrated switch mode BEC with a 5A output at 5V and is compatible with 4S LiPo batteries (Section:3.9). To guarantee durability and dependability, it also offers a variety of protection features such as ESC heat protection and abnormal input voltage.

The ESC controllers work by receiving a digital signal, known as Pulse-Width Modulation (PWM) which have a pulse, the 'width' of these pulses (i.e., how long they stay 'on' versus 'off' in a given cycle) is adjusted to control the speed of the motor. This is known as the duty cycle. A longer 'on' time (wider pulse) means more power is delivered to the motor, making it spin faster. The ESC also includes features like a built-in BEC to power flight controllers and safety protocols for heat and voltage protection, ensuring reliable operation.

### 3.7 Propellers



Figure 3.9: propellers

An essential part that greatly enhances the aircraft's performance and manoeuvrability are the 1045 propellers. This specific quadcopter build is a good fit for these propellers because of their 10 inch diameter and 4.5 inch pitch, which combine to produce a balanced combination of thrust and efficiency.

With '10' denoting the propeller's diameter in inches and '4.5' denoting its pitch in inches, the identifier '1045' describes the propeller's measurements. Understanding the pitch is essential to comprehending the propeller's thrust capabilities and how it will work with the quadcopter's overall aerodynamic design. Pitch is defined as the propeller's theoretical maximum airborne speed in a single rotation, assuming perfect circumstances.

These propellers have a nice balance between strength and weight because they are made of sturdy materials. This guarantees that the propellers can endure the rigours of flight without significantly increasing the quadcopter's total mass, which is crucial for preserving the best possible flight dynamics and battery efficiency

There are two variants for the 1045 propellers: clockwise (CW) and anticlockwise (CCW). This is crucial for quadcopters because, in order to offset the rotational torque generated by each motor and maintain stability and control during flight, each propeller's rotation direction must alternate.

For more information on how these propellers generate thrust, counteract rotational torque and allow for pitch roll and yaw manoeuvres please see Section:2.3

### 3.8 Voltage Regulator



Figure 3.10: Voltage regulator

The Matek Systems Matek - UBEC DUO is a dual-output voltage regulator that offers flexible power management. Wide input voltage range support is provided, and two output channels with substantial power management. While one channel can be adjusted between 5V and 12V to accommodate different components, the other is set at 5V and ideal for receivers or flight controllers.

The GNSS base station module and the flight controller/Raspberry Pi are powered by the voltage regulator on the quadcopter. The GNSS base station is powered by five volts, whereas the flight controller is powered by six, both modules are powered from battery's seen in Figure:3.9.

### 3.9 Battery



Figure 3.11: battery

The GNB 5500mAh 4S 70C LiPo Battery with an XT90 connector is a high-capacity, high-discharge battery designed for use in various remote-controlled (RC) applications. This 5500mAh battery is perfect for long flight times because it keeps a substantial charge and allows for longer use between recharges.

With four cells connected in series, this battery has a 4S1P configuration, producing a nominal voltage of 14.8V. Our high-performance quadcopter needs a lot of power to run due to its weight. This 70C continuous discharge rate shows the battery maintains a steady power flow even while it is under the heavy load of the quadcopter. The battery can safely discharge in this scenario at a rate of 70 times its capacity, or 385A, which provides sufficient power for demanding applications.

The battery also has a burst discharge rate of 140C, which enables brief bursts of even higher power output up to 770A. This feature is helpful in situations where immediate action or rapid acceleration is required. Maintaining performance and safety requires a dependable connection that can handle high current without producing a lot of heat, which is what the XT90 connector offers.

The battery's weight and dimensions are indicative of its high capacity and voltage. Its dependability and longevity are further increased by the inclusion of safety features like short-circuit protection, overcharge and overdischarge prevention, and others. Like this one, the majority of LiPo batteries also include a balancing plug, which is often a JST-XH connector and is used for balance charging. This keeps the battery's general health and efficiency intact by ensuring that each cell is charged equally.

## 3.10 Sensors

This section outlines the various different sensors that were used on the quadcopter, delving into the specs, compatibility and test performance. The analysis includes an examination of the sensors' roles in navigation, stabilization, and telemetry data acquisition.

### GNSS modules

#### 3.10.1 GNSS Rover Module



Figure 3.12: GNSS Rover module



Figure 3.13: Quadcopter antenna

The SparkFun GPS-RTK-SMA Breakout - ZED-F9P Fig.3.12 will prove to be a good option for my onboard GPS module due to its precise GNSS capabilities. It is significantly better than the MikroElektronika GPS Click featuring the LEA-6S, especially in its technical specification. The u-blox ZED-F9P module within, is known for high accuracy and multi- band GNSS support with a maximum update frequency of 25Hz. This allows the quadcopter to utilise real-time kinematic (RTK) positioning which is great for applications which need centimetre level signalling [17]. Ensures comprehensive coverage and reliability due to its ability to access a wide range of satellite systems (GPS, GLONASS, Galileo, and BeiDou). This should prove ideal for getting centimeter accurate data for the quadcopter, hence gaining precise position control on the quadcopter.

To complement the capabilities of the GNSS rover module, it is coupled with the Tallysman 33-SSL889XF L1/L2 GNSS Antenna. This pairing is key to maximizing the performance of the ZED-F9P module, as the Tallysman antenna is designed to optimize signal reception and accuracy for L1/L2 frequencies. Such an integration ensures that the quadcopter benefits from the best possible GNSS performance, crucial for maintaining high precision and reliability in navigation and positioning tasks. This setup is expected to provide the quadcopter with unparalleled precision in its operations, making it exceptionally suited for tasks in accuracy in position control.

For testing evaluation on this module please see Section:5.1

### 3.10.2 GNSS Base Station

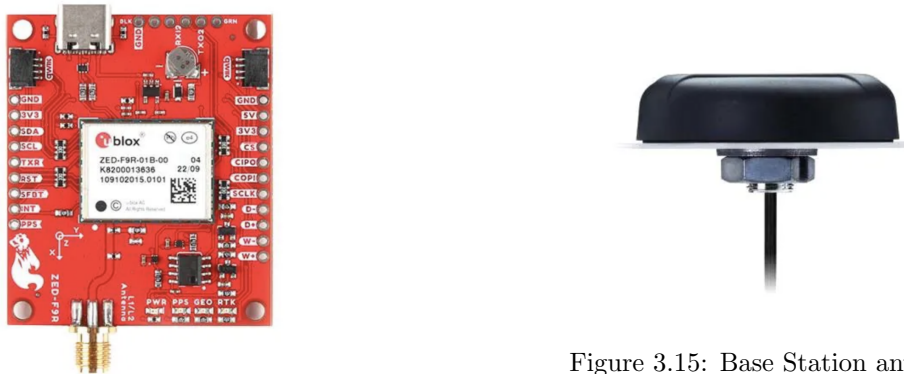


Figure 3.15: Base Station antenna

Figure 3.14: GNSS Base Station module

The SparkFun GPS-RTK Dead Reckoning Breakout - ZED-F9R (Fig.3.14) features make it a highly sophisticated option for GPS-related applications. The modules feature a 184-channel u-blox F9 engine GNSS receiver which will receive signals from GPS, GLONASS, Galileo, and BeiDou constellations with 0.2-meter accuracy with a maximum update frequency of 25Hz. This makes it a superior choice when utilising base station NTRIP technology as well as RTCM (Radio Technical Commission for Maritime Services) messages to communicate correction data to the onboard GNSS module.

The Taoglas A.80 L1/L2 GNSS Antenna is used in conjunction with the GNSS module to support its exceptional performance. This antenna is a perfect fit for the ZED-F9R module because it is specifically made to improve signal reception and accuracy for L1/L2 frequencies. Advanced navigation and autonomous flying systems depend on high positioning precision and dependability, which is ensured by the synergy between the Taoglas antenna and the GNSS module when providing the GNSS rover module above with RTCM correction data. Even in challenging conditions, this combination offers a reliable way to provide exact position tracking and navigation capabilities.

For testing evaluation on this module please see Section:5.1

### 3.10.3 Base station container and stand

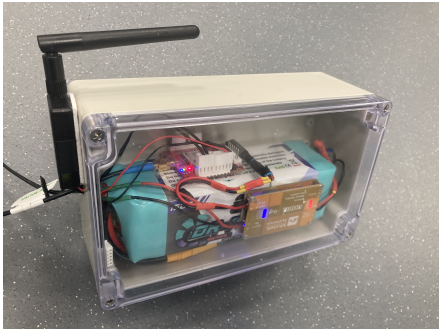


Figure 3.16: Base station container



Figure 3.17: Base station stand with antenna

A container was designed (Figure:3.16) to guarantee the base station's component organisation and water resistance. The GNSS base station module (Figure:3.14), a battery (Figure:3.11), and a voltage regulator (Figure:3.10) were all kept secure from water damage within this container. To ensure clear contact with the GNSS rover module, the telemetry radio—which is essential for transmitting correction data—was placed strategically on the outside (Figure:3.12).

An essential part of the high-performance GNSS base station module is the Taoglas A.80 L1/L2 GNSS Antenna (Figure:3.15). In order to ensure that the base station can efficiently support precise positioning for the GNSS rover module, this antenna was installed on a tripod to secure its position and optimise signal reception (Figure:3.17) for RCTCM corrections.



Figure 3.18: telemetry radio for transmitting correction data

The Holybro SiK Telemetry Radio V3 100mW 433MH 915MHz (Fig3.18) will be used to transmit the RCTCM data from the base station to the on board GNSS module to provide it with the necessary correction data mentioned above. This radio is a lightweight and typically offers a range of over 300 meters. It's important to ensure that the radio telemetry is properly configured to communicate with the GNSS module. This involves setting up parameters such as frequency, power output, and the transmitting of RCTCM data.

### 3.10.4 GNSS Calibration (U-center)

The U-center software, created by u blox is a tool used for setting up, testing and assessing GNSS module data. It offers a range of features to adjust communication ports, protocols, data rates and message settings that are essential, for enhancing the performance of GNSS receivers. Additionally U-center plays a role in updating firmware to ensure GNSS modules operate with the relevant enhancements.

In terms of visuals U-center provides real time data display showing satellite tracking details, signal strengths and other important GNSS information. It presents coordinates, altitude measurements, velocity data and offers detailed insights into the accuracy and reliability of the GNSS data including estimates on positional accuracy. This detailed information is crucial for evaluating the precision and functionality of GNSS modules across applications.

When configuring modules like the SparkFun GPS RTK SMA Breakout. ZED F9P to output GNGGA for altitude and GNGLL for latitude and longitude settings, in U-center involves connecting the module to the software interface. By accessing the Configuration View within U-centers interface users can enable desired NMEA messages while disabling others to streamline output. Saving these configurations in the module's non volatile memory ensures they are maintained through power cycles. When it comes to how updates are made, the SparkFun GPS RTK SMA Breakout ZED F9P and SparkFun GPS RTK Dead Reckoning Breakout ZED F9R can both handle update rates of, up to 25 Hz. This rapid update frequency is ideal for tasks that demand fast results. The ZED F9R, equipped with built in sensors brings advantages for dead reckoning by delivering improved accuracy and consistency even in tough conditions.

To establish a base station that solely outputs RTK corrections you simply need to set the GNSS modules mode to function as a base station choose the RTK correction messages, in this case RTCM3 is used, and specify the output via the correct communication port. These adjustments guarantee that the base station transmits RTK corrections ensuring efficient and accurate data transmission. In order to get the most reliable RTK data from the base station, the 'survey in' feature was used. During the Survey-in process, the base station collects GNSS data over time, and this data is used to calculate a more reliable and stable coordinate estimate of its location. For our particlar use case we wanted the base stations position to be as accurate as possible, in order to achieve this the minimum duration for the survey and the desired positional accuracy were set to 5 minutes and 0.2m, ensuring that the base station's location is determined with high confidence before it begins to transmit the RTK corrections to rover unit.

By integrating these functionalities and setups we can attain high levels of precision and dependability in our GNSS modules, highlighting U-center as a vital tool in satellite navigation practices.

### 3.10.5 Time of Flight sensor



Figure 3.19: Time of Flight sensor

The ToF sensor used to measure the altitude of the quadcopter is shown in Figure 3.19 is the TR-EVO-60M sensor utilises infrared Time-of-Flight technology to detect objects at distances ranging from 0.5 to 60 meters indoors and 0.5 to 10-60 meters outdoors. With an impressive update rate of up to 240 readings per second,

it ensures real-time data collection. Accuracy varies from  $\pm 4\text{cm}$  within 14m to 1.5% beyond 14m, and it provides a minimalist Field of View of approximately  $2^\circ$ . The device requires a 5V DC power supply, with an operational current between 90mA to 330mA. Communication is versatile, with USB, UART, and I2C options available, and it features a Micro USB connector. Its compact dimensions are approximately 29x29x22mm, with a feather-light weight of 9g for the sensor and an additional 3g for the backboard, totalling 12g. The device is also CE certified for eye safety.

### 3.10.6 Barometer



Figure 3.20: Pressure sensor

The BMP180 Digital Barometric Pressure Sensor Module seen in Figure 3.20 is perfect for applications including weather and altitude monitoring due to its compactness, low-power demand and cost effectiveness. It ensures efficiency in battery-powered devices with as little as 0.5 microamperes at 1Hz. With a precision of up to 0.02 hPa—which translates to an altitude detection difference of 17 cm—the sensor offers exceptionally low noise levels. Its pressure measuring range is 300 hPa to 1100 hPa, which allows it to track altitudes from +9000 metres above sea level to about -500 metres below sea level. The module can work between 1.8 and 3.6 volts in the supply voltage range and can communicate at up to 3.5 MHz using an I2C interface.

### 3.10.7 Anemometer



Figure 3.21: Anemometer

For the purpose of detecting wind speed, the quadcopter's sensor package includes an anemometer, The LI-550 TriSonica Mini in Figure:3.21. Real-time wind measurements are essential for the aircraft's stability and manoeuvrability, particularly when performing precise duties like surveying or search and rescue missions [18]. This advanced anemometer, capable of operating within a broad voltage range of 5 - 32 V and consuming a modest power of 400 mW, ensures reliable performance even in the most demanding environments. With

its robust design, the anemometer remains functional at altitudes up to 5000 meters and within a wide temperature range of -20 to 72 °C, making it versatile for various atmospheric conditions.

High-tech instruments called ultrasonic anemometers like the LI-550 TriSonica Mini, are used to measure wind directions and speeds very precisely. The system uses the differential time of flight of ultrasonic pulses between pairs of sensors placed at key angles to function. The device determines wind velocity and bearing by computing the variance when wind modifies the speed of these pulses, with an accuracy of 0.2m/s.

The device's high-resolution wind direction readings, which span a range of 0 to 359°, further highlight its remarkable precision in wind speed and direction measurements and guarantee accurate navigation corrections. Real-time, high-fidelity wind data can be obtained using the anemometer's advanced design, which permits a maximum sampling frequency of 40 Hz and ultrasonic frequency settings around 60 kHz. The anemometer's lightweight design, weighing only 50–67 grammes, ensures that its sophisticated features won't negatively affect the quadcopter's payload.

The sensitivity, resolution, and reaction time of the sensor are critical in delivering real-time analytics for the quadcopter's navigation system and data gathering goals. Therefore, in order to accomplish a thorough analysis and improve the quadcopter's capacity to adjust to abrupt gusts or changing wind patterns, this sensor can provide high-resolution data in three-dimensional space.

### 3.11 Hardware schematic

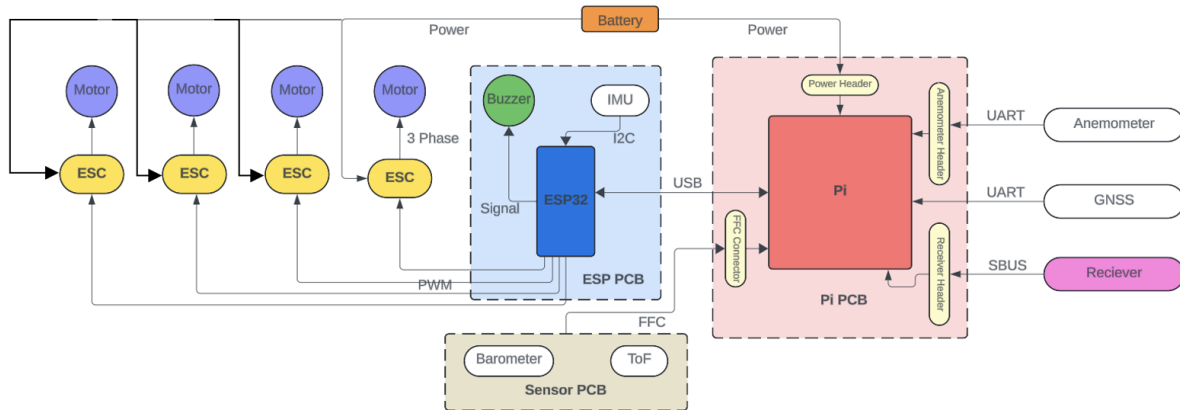


Figure 3.22: Hardware schematic

The hardware schematic above (Figure:3.22) reveals the detailed architecture of a quadcopter's flight control system, highlighting a network of interconnected components orchestrated to ensure optimal flight performance. Central to the above network is the raspberry pi (Figure:3.5), which is the syaytems main computing unit. It interfaces the sensor PCB via a Flexible Flat Cable (FFC) and the ESP PCB via USB, helping to facilitate communication through the system.

In order to power the system, a battery is used (Figure:3.11), this provides the Raspberry Pi and associated components power through the power header on the Pi PCB. The power distribution is crucial for maintaining a consistent electrical flow to the entire system.

For navigation, the Raspberry Pi uses UART connections to communicate with two specialized sensors. One leads to the Anemometer, which measures wind speeds and the other connects to the GNSS rover module, which provides precise location data.

Additionally, the Pi PCB is equipped with an SBUS connection to a receiver. This interface is used to relay remote control commands from a pilot for Pitch, Roll and Yaw manoeuvres or to receive instructions to switch to different autonomous flight modes, thus playing a pivotal role in the control schema of the quadcopter.

The ESP32 microcontroller is mounted on the ESP PCB, which draws power from the system's battery through the Raspberry Pi. It directly manages the quadcopter's propulsion by sending Pulse Width Modulation (PWM) signals to the Electronic Speed Controllers (ESCs). The ESCs then take these pulses and control the motors' speed via 3-phase signals, allowing for precise adjustments to the quadcopter's thrust and direction.

In order for the ESP32 and the Raspberry Pi to communicate, a USB connection between the two is essential for high-speed data exchange between the two processors. The ESP32 also hosts an IMU, connected through the I2C protocol, which feeds the system with motion tracking data for flight stabilization and orientation.

For immediate feedback and alerts, a buzzer is incorporated into the ESP PCB and controlled by the ESP32, serving as an auditory indicator of system states or warnings during flight operations.

Beneath the quadcopter lies the Sensor PCB, strategically placed to minimize interference between the Time-of-Flight (ToF) sensor and Barometer and the other components, as well as for getting reliable data from the ToF sensor as it needs a clear view of the ground. This PCB is connected through a FFC, this design choice underscores the importance of unimpeded sensor functionality, as the ToF and Barometer provide critical altitude measurements for control.

The schematic layout presented in Figure:3.22 above encapsulates a meticulously designed system where power, control, and data harmoniously converge to create a responsive and efficient flight control ecosystem. Every component and connection is deliberately positioned to contribute to the quadcopter's agility, stability, and navigational precision, reaffirming the system's engineering sophistication.

## 3.12 Cost of materials

### Main Parts

Part	Quantity	Approx. Price (£)
DJI F450 Frame	1	20
PROPDIVE v2 3536 1400KV Motor	4	75
Skywalker 50A ESC's	4	70
1045 Propellers	1	13
Landing Gear/Frame legs	1	4
Shock Absorber Anti-vibration	1	5
Pool Noodle/quadcopter feet	1	15
RadioLink AT10 II RC + R12DS Receiver	1	120
LiPo Battery GNB 5500mAh 4S 70C (XT90)	as req.	(each) 50
LiPo Battery GNB 7000mAh 4S 70C (XT90)	as req.	(each) 60

Table 3.2: List of main hardware parts to build the quadcopter

## Electronics

Part	Quantity	Approx. Price (£)
Raspberry Pi 4B 4GB	1	55
ESP32 Dev	1	14
SanDisk 128GB USB	1	14
MPU9250 IMU	1	5
Terabee TR-EVO-60M-I2C (ToF)	1	113
BMP180 Pressure Sensor	1	3
Carbon Kevlar Tube	1	32
TriSonica Mini LL-550P Anemometer	1	(Ask for Quote) 2065
SparkFun ZED-F9R GNSS Module (Quadcopter)	1	230
Tallysman 33-SSL889XF L1/L2 GNSS Antenna (Quadcopter)	1	150
SparkFun ZED-F9P GNSS Module (Base station)	1	220
Taoglas A.80 L1/L2 GNSS Antenna (Base station)	1	90
Male SMA Cable (cut to length)	1	7
MMCX Connector (solder to above)	1	7
USB A to USB C (Quadcopter)	1	8
UBEC Voltage Regulator	1	20
HOLYBRO - Telemetry Radio Set	1	65
UBEC Voltage Regulator	1	20
USB A to Micro USB	1	6

Table 3.3: list of electronic parts needed to build the quadcopter

## Others

Part	Approx. Price (£)
Lipo Battery Charger	37
XT90 Connector to Banana Plugs	8
Lipo Safe Bag	16
1-8S Cell Checker with Alarm	3
TP-LINK Sim Wi-Fi Router	120

Table 3.4: Other parts to consider purchasing when building the quadcopter

In conclusion, the parts list above indicates an approximate total cost of £3730 for creating the quadcopter. This estimate does not include additional costs for PCB design, wiring, connectors (e.g., nuts and bolts), or any necessary 3D printed components. It is based on the assumption that a minimal quantity of batteries will be purchased. It's crucial to remember that actual pricing could change based on changes in the market, delivery charges, and any possible discounts for large purchases. While this offers a useful starting point for budgeting, builders should be ready for possible fluctuations in the final overall cost. It's also advised to think about setting aside money for unanticipated costs or modifications that could improve the quadcopter's functionality.

### 3.13 PCB design

#### Formation of the flight controller

In order to form the flight controller, Two PCB's were designed one for Anemometer, GNSS and Receiver connections depicted above in figures:3.23 and 3.24, and the other for mounting the IMU and ESC connections, depicted in Figure:3.26.

##### 3.13.1 Raspberry Pi PCB



Figure 3.23: Pi PCB (bottom)



Figure 3.24: Pi PCB (top)



Figure 3.25: Pi PCB attached to Pi

The custom designed Raspberry Pi shield is shown in figures:3.23 and 3.24. The radio receiver is connected to the Raspberry Pi GPIO via an SBUS connection in this circuit and the Anemometer and GNSS connections via UART. The Raspberry Pi's I2C and UART communication pins are linked to a IDC ribbon cable connector for communication with the sensor PCB, see Section:3.13.3.

The mounting holes at the four corners of the PCB are used to fasten the board to the Pi after it has been plugged into the Pi's GPIO pins. This is depicted in Figure:3.25

### 3.13.2 ESP PCB



Figure 3.26: ESP32 PCB with IMU attached

The ESP shield is a custom designed PCD for electrical designs on the ESP32 WROOM board. All of the connections required to link the ESP and IMU via I2C are included in the circuit. It additionally allows the ESP to connect to the ESCs and a buzzer. The ESP shield is depicted above in Figure:3.26.

The ESP, the IMU, and the buzzer can all be accommodated on the board. Furthermore, every unassigned pin is now connected to one of three ports; PORT 1, PORT 2, and PORT 3, respectively. Four mounting holes on the board line up with the Pi's mounting holes, depicted in Figure:3.27.

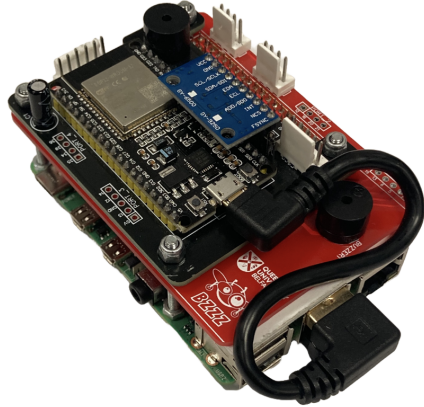


Figure 3.27: Flight controller

After the flight controller is assembled, we have a powerful system that serves as the basis for the quadcopter's functional abilities. The Raspberry Pi shield guarantees reliable device interface thanks to its strategic placement of connections to the radio receiver, GNSS and Anemometer. Essential GPIO pins through an SBUS and an IDC ribbon cable connector for the ToF and Pressure sensor (see Section:3.13.3). the ESP32 shield is carefully designed to fit both the ESP module and the MPU9250 IMU. For increased connectivity choices, each unallocated pin is systematically attached to one of the three available ports (PORT 1, PORT 2, and PORT 3). The USB connection between the Raspberry Pi and the ESP32 completes this assembly and provides a dependable, fast communication channel that is essential for the interchange of control and sensor data.

### 3.13.3 Sensor PCB

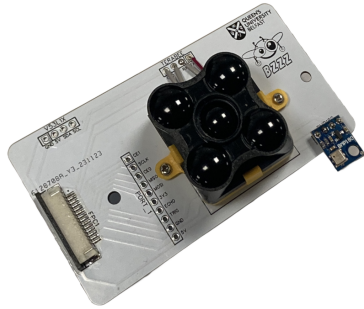


Figure 3.28: Sensor PCB, including ToF and Barometer sensors

The sensor PCB is designed to be installed at the quadcopter's base attached to the baseplate. By ensuring that the Time-of-Flight (ToF) and Barometer sensors are exposed to the environment without obstruction, a crucial aspect for accurate measurements, this placement optimises their operation. The sensors are positioned strategically to reduce interference from other electronics and to provide a steady platform for the correct collection of altitude data, which is essential to the flight control system. The method of establishing communication between the Raspberry Pi and the Sensor PCB involves attaching a Flexible Flat Cable (FFC) to the IDC ribbon cable connector. The ToF sensor is attached via bolts and the barometer is soldered on.

### 3.13.4 Power Distribution PCB

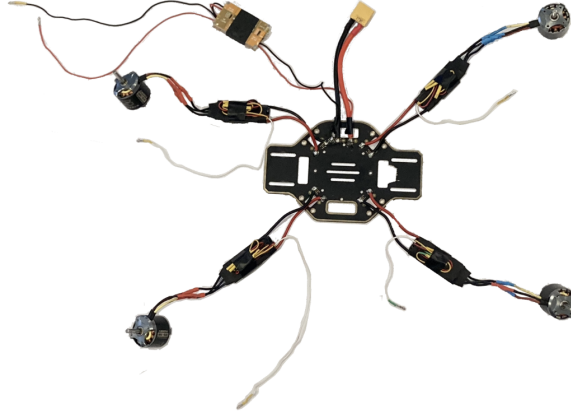


Figure 3.29: Power distribution board

The power distribution PCB depicted above in Figure:3.29 is the central hub for distributing powers across the quadcopter. Each Electronic Speed Controller (ESC) is connected to the PDB, which receives power from the main battery. The ESCs then regulate the power to the motors, adjusting speed and rotation based on the control signals received, via PWM (Pulse Width Modulation) from the flight controller.

The ESCs are essential for supplying the controlled, variable power required for the exact movements of the quadcopter. They are coupled to their respective motors. The quadcopter's manoeuvrability is made

possible by the ESCs, which make sure the motors react appropriately to inputs from the flight controller. The PDB guarantees that all the electronic components receive the power they require.

Stable power delivery to the flight controller is ensured by the voltage regulator, which is essential for its computational tasks and stability functions. It powers vital navigation and control systems, such as the GNSS module, IMU, Anemometer, ToF sensor and Barometer, by converting the battery's fluctuating voltage to a constant level, which helps the quadcopter fly precisely and steadily.

# Chapter 4

## Software

This project's code is all located in one repository on GitHub. The purpose of a central platform for version control and communication is served by the repository. The extensive documentation to help developers understand and contribute to the project is available in the repository. Its methodical arrangement makes it simple to navigate through a variety of components, such as control systems, Kalman filters, and sensor integration.

My project involvement has also seen me contribute to the features that allowed the interpretation of GNSS data that translates the satellite signals into usable location information for the quadcopter. I interpreted barometer data that gave the altitude from pressure readings, Kalman filter design. I took charge of setting up all sensors in the system paving the way for sensor fusion and data amalgamation.

I gave clear explanations and usage guidelines for our Kalman filter, to make the system easier to understand and use, setting the ground for further enhancements. I have accomplished the development of the Kalman filter itself by using simulators I found the optimal tuning values for performance of the Kalman filter in the Altitude and Position control tasks. I designed a PID controller for the Positioning control and a PD controller for the altitude control with the Kalman filter for the sensor fusion, determining accurate functionality was achieved through simulation design. This underscores the projects dedication to responsive control mechanisms.

These contributions demonstrate my involvement, with the project and dedication to enhancing the capabilities of this system while aligning with my project objectives.

## 4.1 Main Loop

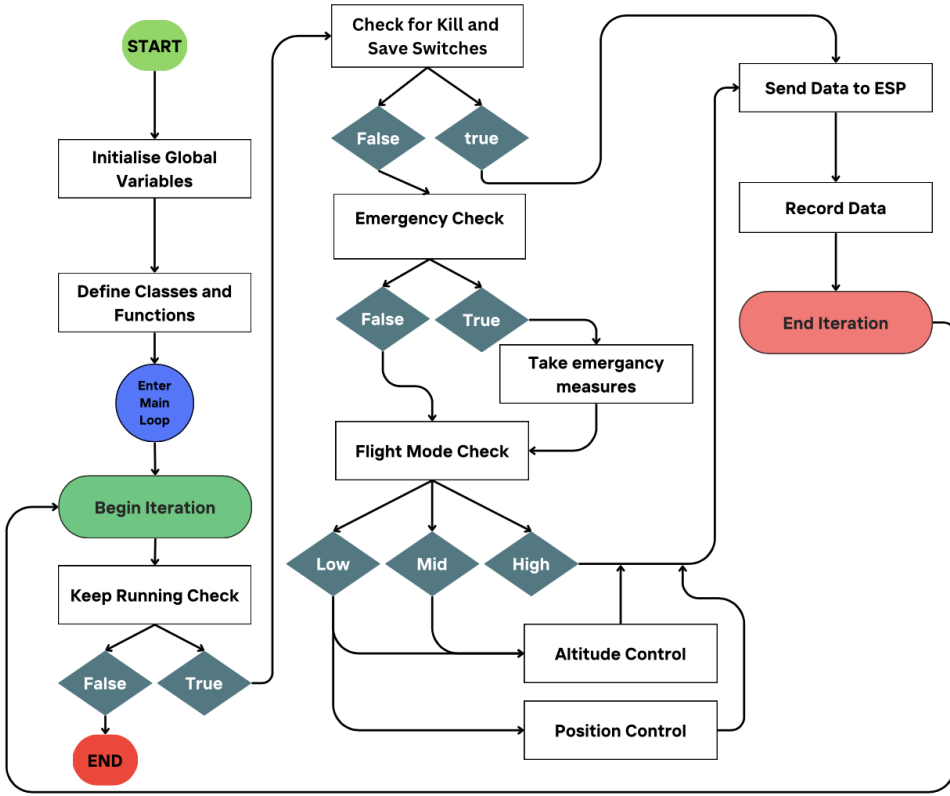


Figure 4.1: Main loop flowchart

The quadcopter control programme starts by configuring the necessary runtime environment, which includes initialising global variables and parameter configurations that are essential for flying operations. During this stage, the system loads vital values from a preset constants module, like the minimum altitude required for altitude hold and sensor calibration data. Furthermore, instances of the DataLogger and AltitudeHold-KalmanFilter classes are brought in, in order to offer real-time data logging and altitude estimate capabilities.

Once all necessary classes and functions have been defined, the system enters its main operating loop. The constant processing of actuator commands and sensor readings forms the core of the control system, represented by this loop. At the beginning of each iteration, a conditional flag that indicates whether the loop should continue is checked. The 'Keep Running Check' looks for unexpected behaviour or outside orders to halt processes. In order to make sure the software can seamlessly exit the loop when necessary, it verifies user inputs from the RC and analyses the present state of the system.

The 'kill' and 'save' switches in the RC (Remote Control) class are checked as part of the flight control logic. In unwanted situations, it enables the user to command the system to store flight data records or to stop the entire flight. In the event that the quadcopter loses communication with the remote controller or is 'killed' above a predetermined height, the software initiates a 'Emergency Check' to determine whether prompt safety measures are required. These measurements are based on real-time sensor data from the Time of Flight sensor. To put emergency responses into action, utilise the take emergency measure function. The likelihood of the quadcopter crashing is decreased by taking various actions, such as adjusting the throttle

for a controlled landing, depending on how serious the issue is.

In addition, the control system carries out a 'Flight Mode Check', in which it uses the input from the RC class to determine the proper control response, such as position control or altitude hold. If the quadcopter is in the proper state ,the AltitudeController and PositionController classes are used to calculate the necessary control signals based on the feedback from location and altitude sensors. These particular controllers are a crucial component of an intricate PD and PID systems that dynamically regulates propulsion on all axes to allow the quadcopter to fly in the correct direction.

Communication with peripheral modules are handled by the EspBridge class, which serializes control and telemetry data and transmits it to the ESP module for further communication or processing. Moreover, the data obtained during the flight is stored using the DataLogger class that records time-stamped sensor readings alongside the control commands. This will be utilised as a black box record that is critical for post-flight assessment and provides invaluable analysis for enhancements.

The classes demonstrate that the system was developed with concurrent operation in mind. By handling sensor data acquisition in parallel to the primary control loop, the ToF, pressure sensor and Gnss classes reduce the amount of influence latency has on controller responsiveness. To ensure the integrity of sensor data required for control decisions and to avoid data races, these classes employ thread locks to synchronise access to shared resources. In addition, the DataLogger class was crafted such that the act of recording data has no effect on the main control loop's performance.

In conclusion, a well-designed set of checks and controls throughout the quadcopters control system architecture allows for a secure and stable operation. The quadcopters software conducts precision flight control yet maintains an unwavering interest in safety through constant real-time monitoring and management of contingencies. The multi-threaded architecture and asynchronous processing of sensor data gathering highlight the system's efficiency in a real-time setting, indicating a system prepared to withstand the demanding requirements of aerial operations.

## 4.2 Sensor Data Acquisition

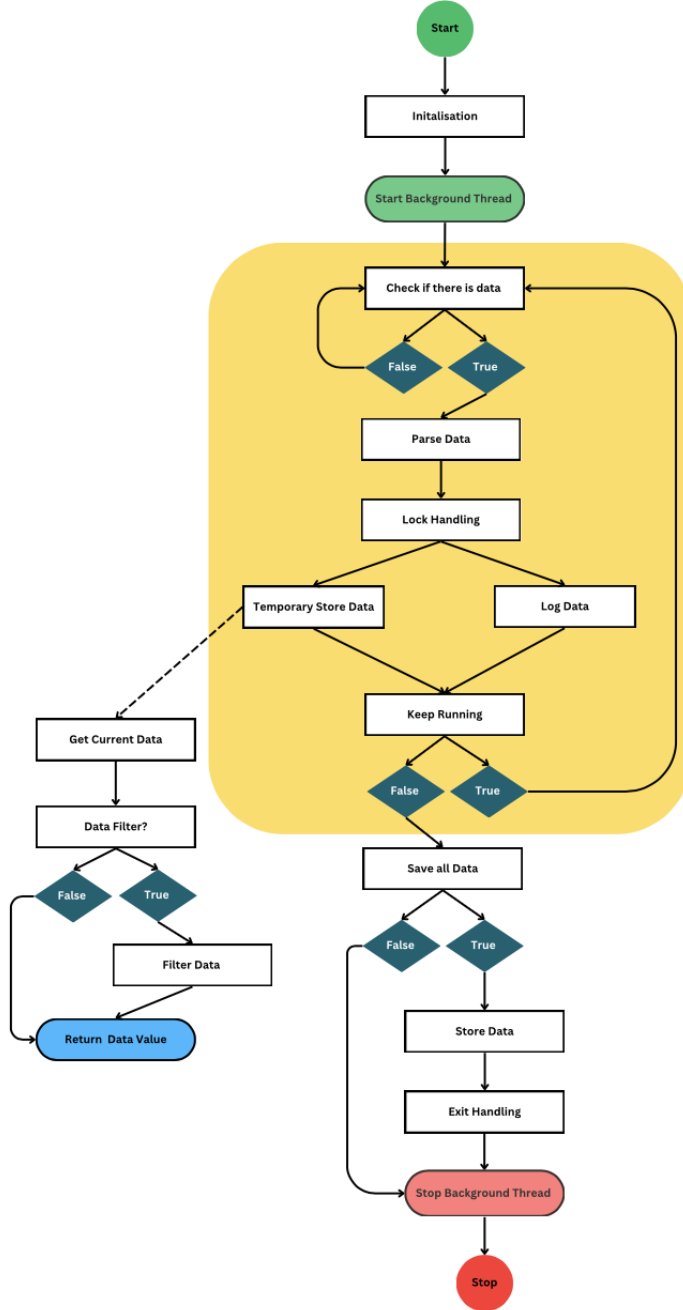


Figure 4.2: Sensor flowchart

The technical execution of the sensor data processing system begins in the initialization phase: it involves configuring global variables and creating a framework for data collecting. The sensor class's are set up in this phase to specify the window length for data processing, establish the serial channel and baud rate for transmission, and, if necessary, instantiate the median filter and data logger.

The system launches a background thread following the successful completion of the initialization step.

This is essential to the system's capacity to carry out asynchronous operations. The thread's job is to read data from the sensor at all times, working autonomously and without interfering with or disrupting the main control loop.

The system ensures that data access is thread-safe by applying a lock mechanism the system defines a lock state, which prohibits simultaneous write/read operations that can lead to data corruption. Its key action in the control loop is to periodically check the serial buffer for new data. If new data are identified, the raw data is read, processed, and converted into a format that can be used to describe the sensor measurements like distance/altitude. The parsed data is temporarily stored in an array, maintaining the synchronization guaranteed by the lock to ensure that multi-threaded operations always preserve data consistency.

Another critical function in the control loop is data logging. If active, the quadcopter's sensory inputs create a permanent record by adding each sensor reading, which is perfectly timestamped, to a log file in csv format. This data is critical for post-flight analysis. Furthermore, a conditional filter check is appended to decide if it is necessary to perform additional processing on the newly acquired data to reduce noise or outliers. When filtering is necessary, ta Median Filter analyses the data that has been stored and returns a refined value that the system may use.

In the main loop, a 'Keep Running' check determines whether or not the system should keep running. When a user tries to end a flight, such as when they activate the 'kill' or 'save' switches, the code will be broken out of this loop. In the event that the exit condition is satisfied, the system immediately saves all of the gathered data in order to prevent data loss. This safeguard comes before the organised method of leaving, which includes terminating the background thread. This methodical exit procedure guarantees a secure termination by ensuring that all tasks are completed smoothly, that the data is saved, and that the system resources are freed.

The system enters a halt state and stops all operations in the last phase. The program's execution thread cycles comes to an end with this step. Therefore, mentaining data safety when terminating the quadcopter.

# Chapter 5

## Tests

### 5.1 GNSS rover module test, with correction Vs without

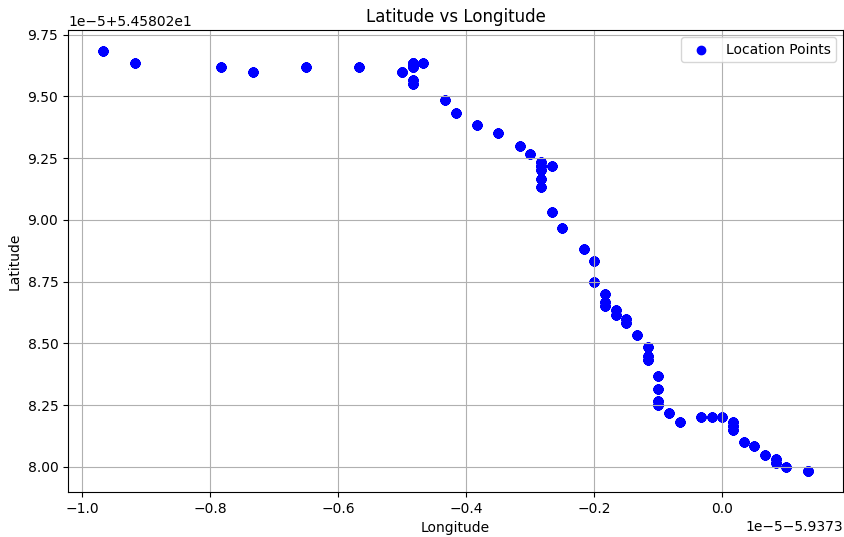


Figure 5.1: GNSS readings without the use of RTK corrections form the base station

```
Latitude Range: 1.699999999971169e-05
Longitude Range: 1.0999999998873022e-05
Latitude Range in Meters: 1.8869999999679976
Longitude Range in Meters: 0.7076446726772408
Maximum Range in Meters: 2.015323791019126
Number of Unique Positions: 59
```

Figure 5.2: GNSS Percesion Data (Without corrections)

In the figures above, Figure:5.1 and Figure:5.2 represent the GNSS latitude and longitude recorded while the module remained in a fixed position. The purpose of this setup was to calculate the overall precision of our GNSS module without the correction data streaming from the base station.

From the above graph in Figure:5.1 we can see that the recorded longitude and latitide points are drifting. Ideally, when a GNSS module is fixed in one position, it would be expected that the recorded latitude and longitude data points to cluster tightly around a single coordinate pair, indicating a high level of precision. However this is not the case as the spread of data points seen here suggests a certain level of positional inaccuracy, this is due to the fact that the module is not availing of the RTK correction stream from the GNSS base station we have set up.

Figure:5.2 shows a terminal output from the python code written to summerise the data recorded. From this we can see that the range of values of longitude and latitude readings, converted to meters are, 1.887m (3.d.p) and 0.708m (3.d.p). Next the overall max and min points on the graph are calclulated using Pythagorean theorem showing that the readings span over 2.015m (3.d.p) accross 59 readings.

In Conclusion, the test results show that, the accuracy of GNSS data is limited and are not be suitable for applications that require high precision. The variations in data points and observed drift indicate that the GNSS modules accuracy fluctuates, potentially affecting its reliability when used in position control on the quadcopter. With a dispersion of 2.015 meters across 59 readings it is clear that using RTK corrections is essential for getting more accurate data. While the GNSS module offers location information it falls short in meeting the precision requirements whitch are needed for accurate position control.

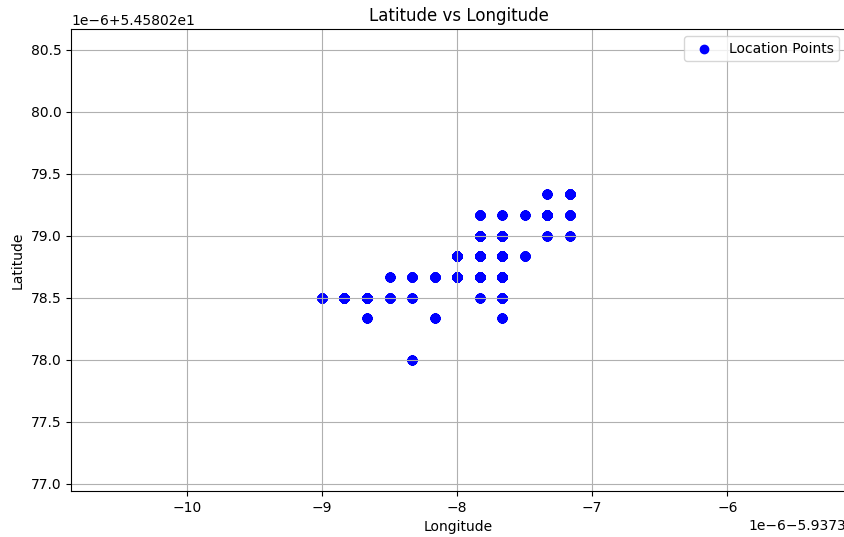


Figure 5.3: GNSS readings with the use of RTK corrections form the base station

```

Latitude Range: 1.333333299669903e-06
Longitude Range: 1.833333322573253e-06
Latitude Range in Meters: 0.1479999962633592
Longitude Range in Meters: 0.11794080687538204
Maximum Range in Meters: 0.18924596116116083
Number of Unique Positions: 32

```

Figure 5.4: GNSS Percesion Data (With corrections)

In the figures above, Figure:5.3 and Figure:5.4 represent the GNSS latitude and longitude recorded while the module remained in a fixed position. The purpose of this setup was to calculate the overall precision of

our GNSS module without the correction data streaming from the base station.

From the above graph in Figure:5.3 we can see that the recorded longitude and latitide points are in a distinct cluster. Due to the fact that RTK corrections have now been streamed from the base station there is less variation in readings, indicating a high level of precision.

Figure:5.2 shows a terminal output from the python code written to summerise the data recorded. From this we can see that the range of values of longitude and latitude readings, converted to meters are, 0.148m (3.d.p) and 0.118m (3.d.p). Next the overall max and min points on the graph are calclulated using Pythagorean theorem showing that the readings span over 0.189m (3.d.p) accross 32 readings.

In conclusion the use of RTK corrections has proven vary useful, shocasing values of high percision, which is needed for position control on the quadcopter. There is little variation in data points with a dispersion of 0.189 meters across 59 readings, when copared to 2.015 meters in the test above it is undeniable the significant enhancement in accuracy achieved through ustalizing RTK corrections.

## 5.2 Testing of Kalman filter

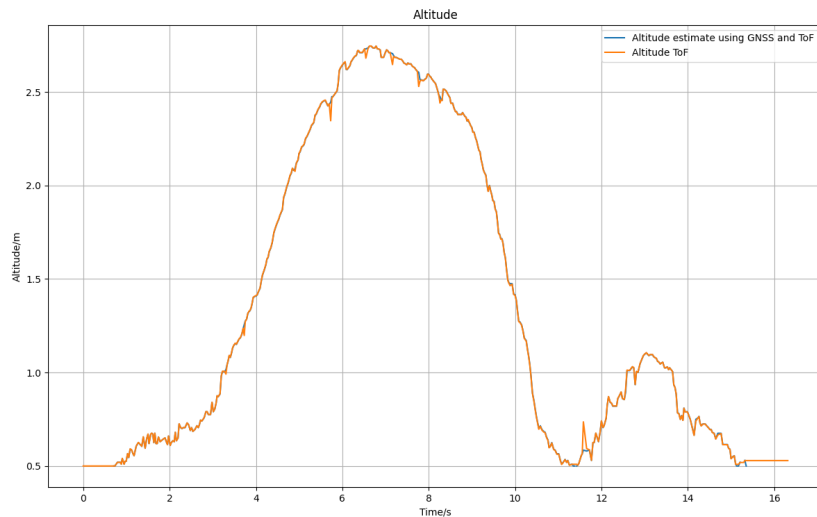


Figure 5.5: Time of Flight sensor vs sensor fused Kalman filter with GPS and ToF data

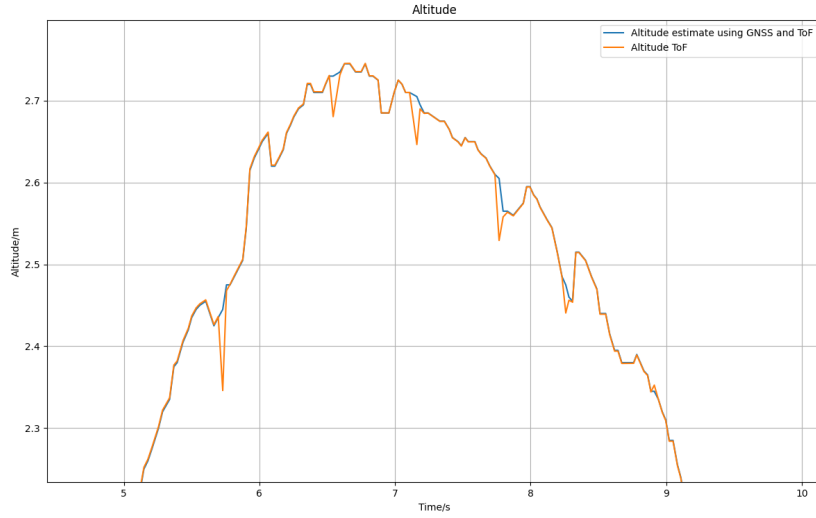


Figure 5.6: Time of Flight sensor vs sensor fused Kalman filter with GPS and ToF data zoomed

In this test the quadcopter was briefly flown in order to test the kalman filter and how well it filters noisey data when compared to using the ToF sensor by itself.

From Figures:5.5 and 5.6 we can see that the kallman filter does a good job at filtering out the noisey data smoothing out the curve of altitude measurments.

This is especially usefull when it comes to flying over uneven terrain such as long grass where using the ToF sensor alone will introduce inaccuracys in the altitude measurements.

### 5.3 Testing initial estimate for $\alpha_0$ and $\beta_0$

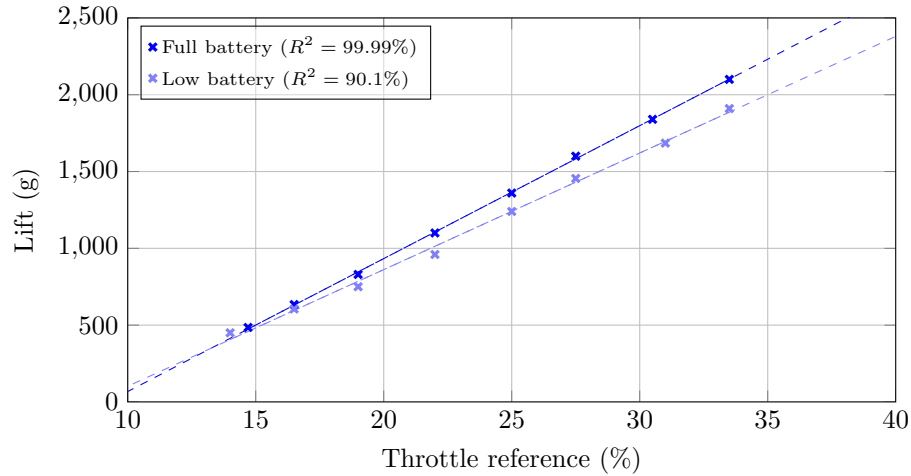


Figure 5.7: Static lift (g) plotted against throttle reference (%).

The quadcopter was placed on digital scales ontop of a platform to minnimize ground effect, and the lift (in g) was measured for different values of  $\tau$ . The experimental results are shown in Figure:5.7, the

graph shows a clear linear relationship between the throttle reference and the static lift produced by the quadcopter. There are two sets of data represented by two different linear fits: one for when the battery is full and another for when the battery is low.

From the trendlines in the graph the derived model for the lifting force is  $F_{\text{prop}} = \alpha_0\tau + \beta_0$ , where  $\alpha_0 > 0$  and  $\beta_0 < 0$  are constants, which depend on the level of charge of the battery.

- **Full Battery:** The graph shows that the quadcopter has a relatively constant lift force across various throttle references when the battery is fully charged. The high  $R^2$  value of 99.99% which indicates an almost perfect linear correlation, is evidence of this. When the battery is fully charged, the slope of this line would be  $\alpha_0$  and where the line intersects the y-axis (lift) is  $\beta_0$ .
- **Low Battery:** The slope of the line becomes less steep when the battery is low, indicating that  $\alpha_0$  is smaller when the battery is low than when it is full. Additionally, the  $R^2$  value is lower (90.1%), indicating a less consistent relationship that may be caused by variations in battery performance as the charge decreases. again where the line intersects the y-axis (lift) is  $\beta_0$ .

In conclusion, the values for  $\alpha_0$  and  $\beta_0$  were found to be 8654 and -797.67 respectively. These values were then used in equations:2.19 and 2.20 for deriving the initial values for  $\alpha$  and  $\beta$  in the Kalman filter.

## 5.4 Altitude control

### Altitude control whilst quadcopter is static

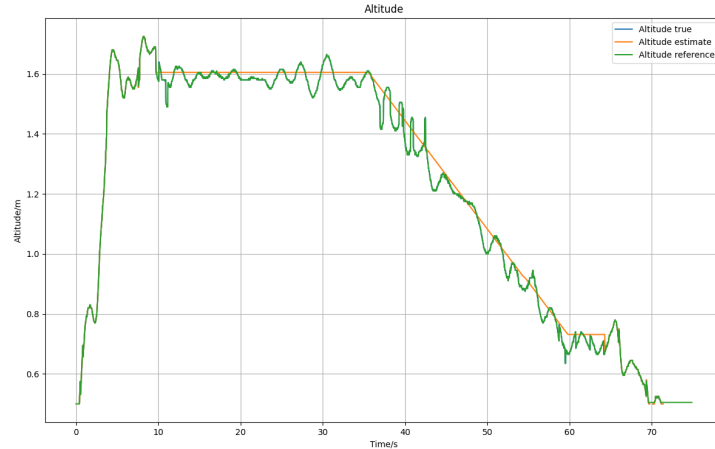


Figure 5.8: Altitude control whilst quadcopter has little horizontal movement

In this test shown in Figure:5.8 took place indoors using the Time of Flight (ToF) sensor only, the Quadcopter is taken off in manual flight mode as usual once a steady altitude was found using the throttle on the remote, the altitude control mode was initialised using the RC. The altitude trimmer was then used to lower the altitude refference until it was low enough to land in manual mode. In the graph the Green line represents the true altitude from the ToF sensor, the Orange line represents the refference altitude. From the above graph we can see that the quadcopter performs well in a controlled osolation around the refference point of

$\pm 10$  centimeters thought. The quadcopter behavior demonstrated a well tuned PD controller with a P gain of 0.5 and a D gain of 0.07, this control proved impressive as it was able to follow the refference altitude down as the trimmer was decreing, mentaining the same accuracy as before in a consistant altitude. The lack of spikes in velocities seen in the altitude control portion of the graph proves impressive when compared to manual mode, showcasing the its persise control over the quadcopter.

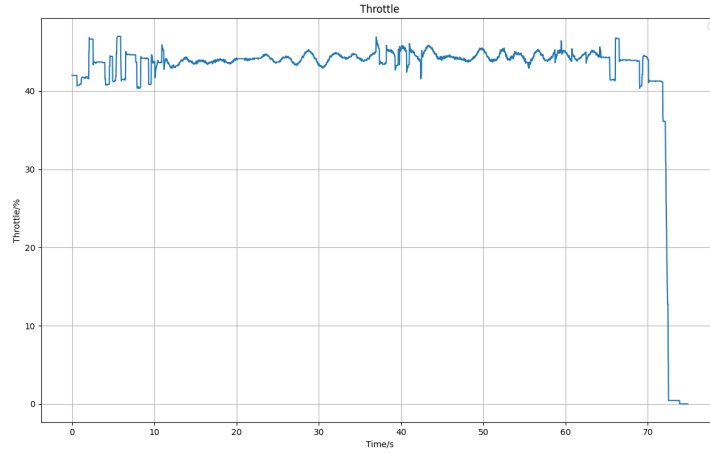


Figure 5.9: Throttle measurments in Altitude control mode whilst quadcopter has little horizontal movement

The graph above (Figure:5.9) depicts the throttle percentage readings against time. The graphs shows continuously smooth throttle changes when the altitude refrence is not being changed, followed by a slight osolation when the refference is lowered gradually. This inaccuracy is then mitigated as the altitude converges back on the refference altitude.

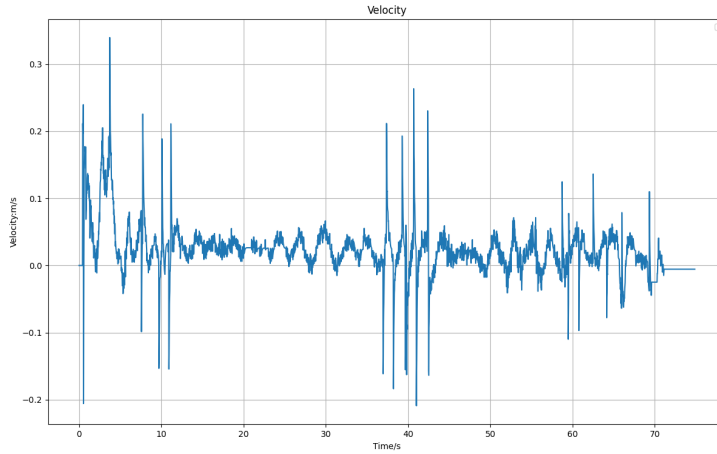


Figure 5.10: Velocity measurments in Altitude control mode whilst quadcopter has little horizontal movement

When analysing the velocity graph in the test (Figure:5.10) it can be seen that the velocity of the quadcopter is emediately smoothed when altitude control mode has been initilised around the 10 second

mark. The velocity of the quadcopter continues to stay smooth until the altitude reffernce is lowered causing some inaccuracy followed by a further conversion velocity as the true altitude gets closer to the refferance altitude.

In conclusion the quadcopter's performance in the altitude control mode, as shown in this test, was deemed exceptional. The altitude accuracy of  $\pm 10$  centimetres from the reference altitude shows that the system is capable of exceptional control using a PD controller even when the refference altitude is being altered. Hence this test proves the quadcopter to be a good solution for many different applications of aerial control such as, photography, surveying and search and rescue.

Furthermore, It could potentially be further improved with additional calibration of the P and D values in the controller, this will take further time and testing.

### Quadcopter moving whilst in altitude control mode

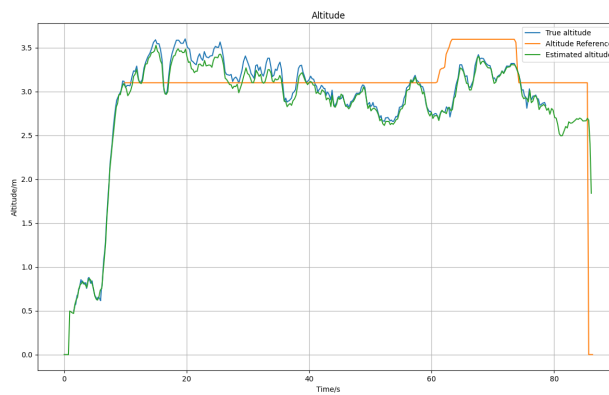


Figure 5.11: Altitude control test whilst quadcopter is moving

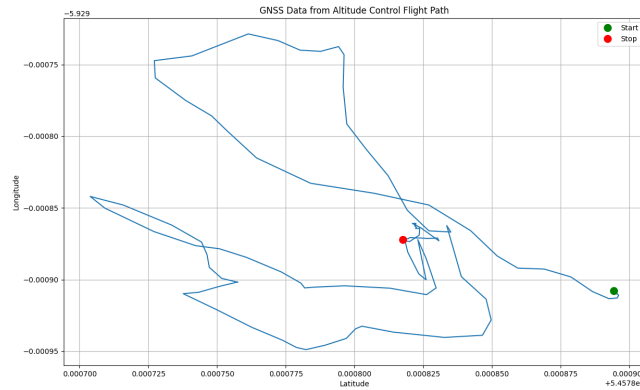


Figure 5.12: GNSS Data from Altitude Control flight path

In this test, the quadcopter was taken off and landed as normal. During the flight the altitude control feature was initialised on the quadcopter and flown the quadcopter, flying in a radius of around 10m, shown in Figure:5.12.

Figure:5.11 illustrates the quadcopters altitude in orange, refferance altitude in green, throttle signal in red and the velocity in blue.

It is crucial to take into account the circumstances and external influences that might have affected the recorded outcomes when assessing how well the quadcopter's altitude control capability performed. The quadcopter flew with an altitude accuracy of about  $\pm 30$  centimetres from the reference altitude of 3.1m, as stated in the test description. This indicates a reasonably stable performance while operating in the altitude control mode. This degree of accuracy is impressive, especially in light of the difficulties caused by outside variables like strong winds and the dynamics of the quadcopter's motion.

As the test continues the altitude trimmer on the side of the remote was increased, this in turn gradually increases the refferance altitude. From the graph we can see that the quadcopter successfully reacted to this change in refferance, furthermore showcasing the quadcopers control algorithms abilities.

The disparity in altitude control, as seen in Figure:5.11,can be linked to the high wind velocity that was present throughout the test. Because wind exerts unpredictable forces on the quadcopter, it can create significant unpredictability in altitude control, making it more difficult to keep a steady altitude.

Furthermore, altitude control may become even more challenging due to the quadcopter's movement, particularly when it involves pitch and roll changes. A forward/backword pitch or left/right roll can cause a drop in altitude if it isn't corrected for by increasing the throttle, as Figure:5.13 shows bellow. This is due to the fact that when the quadcopter is tilted forward or sideways for movement, it directs some of the thrust horizontally, thereby reducing the vertical thrust component that counteracts gravity. In such cases, in order to maintain the required height, the altitude control system has to dynamically adjust the throttle which can cause the controller to osolate between movements. In order to fix this problem the relevant pitch and roll angles should be parsed from the IMU, these angles should them be used in the basic trigonometry equation  $a = \text{recorded}_{\text{altitude}} \cdot \cos(\theta)$  where  $a$  is the true altitude and  $\theta$  is the recorded angle from the IMU.

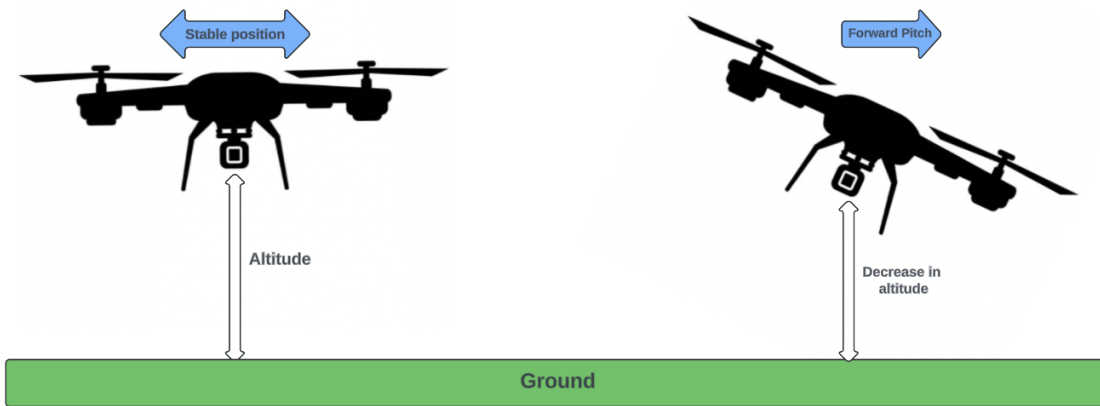


Figure 5.13: Moving quadcopter causing an decrease in altitude if throttle percentage is kept the same

In light of the operational and environmental difficulties encountered, the quadcopter's performance in the altitude control mode, as proven in this test, was deemed good. Even if there is still space for development,

the altitude accuracy of 0.6 metres from the reference altitude shows that the system is capable of handling external elements like wind and movement dynamics. It can be further with additional calibration of the P and D values in the controller. The altitude control capability will need to be continuously improved and tested in a variety of scenarios in order to function more precisely and consistently.

# **Chapter 6**

## **Reflection on progress**

### **6.1 Time analysis**

In the Time analysis segment, systematic analysis of the various aspects of the bzzz project, detailing the duration and sequencing of the developmental phases, implementation, and testing of the bzzz quadcopter. The meticulous break down of time allocation for each task in the project, highlighting efficiency gains and bottlenecks encountered.

Below in figures:6.1 and 6.2 is the gantt chart and key provided in the Intrim report:



Figure 6.1: Gantt chart



Figure 6.2: Gantt chart key

## Steps within time constraints

The parsing of GNSS data as well as testing the code was a notable success, our results demonstrated the codes ability to efficiently manage to extract and interpret the GNSS data streams using multi threading, parsing Latitude, Longatitude and Altitude data, which are crucial for the quadcopter's navigational systems. The success in this area was due to the extensive research that was done in GNSS data strings prior to writing the code.

The GNSS rover module testing proved to be a strong point, offering insightful information on the system's performance and capabilities in real-world scenarios. A number of successful trials that verified the module's functionality and reliability for more integration with the UAV system were made possible by the well-organized testing processes.

Controller research also progressed within the allocated time constraints, exploring various control strategies that could be applied to the bzzz quadcopter. Due to this extensive research it was determined that a PD controller for altitude control and a PID controller for position control was most applicable. The derived plan from the research paved the way for a quick turnaround when it came to simulating the controller.

Finally, designing simulations for the kalman filter progressed well, this was due to the fact that extensive documentation was written prior to designing these simulations. This documentation layed the groundwork for simulation implementation providing great results from the get go meaning that little tuning was needed, allowing for a quick turn around.

## Steps outside time constraints

The Design of the kalman filter documentation persisted challenges, taking longer than expected. The complexity of the mathematical modeling required a more extensive developmental phase to ensure the filter's accuracy and reliability when it came to making simulations and overall implementation. On the other hand the extended time spent writing the detailed documentation on the filter was made up for when designing simulations and overall implementation as it paved the way for these processes.

The decision to implement a base station introduced unexpected complexities into the system architecture. This meant having to do further research into calibration, figuring out a way to broadcast the correction data from the base station to the rover module, designing a water resistant casing and finally the design of the station that allowed for portability.

Testing setbacks for altitude control were encountered due to unfavorable weather conditions and an unfortunate incident of crashing. These external factors meant that this process took longer than anticipated.

Lastly, the PD control implementation for altitude control faced hurdles. The iterative process of tuning the PD parameters to achieve the desired level of control and stability took additional time. Although

the simulations provided promising results they were not directly transferable to real life conditions due to several factors such as weight and environmental conditions.

## 6.2 Objective analysis

Upon starting this project objectives were laid out as well as the learning outcomes, as seen below,

### Objectives

1. To design, implement and test a Kalman filter to estimate the (x, y, z)- position and the heading of the quadcopter using information from the IMU, the altimeter, and a GPS module.
2. To design, implement and test a control system for loitering.
3. To perform certain hardware tasks (proper mounting and connection of the GPS module to the on-board Raspberry Pi)
4. To perform experiments and record flight data

### Learning Outcomes

1. Have mastered the theory of LQR and Kalman filtering.
2. Understand how a GPS module works and be able to interface it.
3. Be able to design a PCB.
4. Have a solid understanding of the attitude and translational dynamics of a quadcopter.
5. Be able to perform simulations of dynamical systems in Python.
6. Be able to operate a quadcopter using an RC.
7. Be able to integrate different systems involving hardware and software components.
8. Be able to use git and GitHub (branches, pull requests, etc).

### Objective 1

The Projects first objective was to design a Kalman filter to estimate position on all axis using the information from various different sensors. This objective was satisfied by my robust kalman filter design seen in Section:2.4.3. Using Sensor fusion the kalman filter was developed to incorporate information from the GNSS module, Tof sensor and barometer. The integration described allowed for centimeter level accuracy in altitude control (seen in Section:5.4), demonstrating the high level of engineering and strong algorithmic design which back the filter. Reliable data from the GNSS module, Tof sensor and barometer data parsing classes were imputed into the filter, this along with the meticulous calibration and fine-tuning of the filter parameters led to improved flight stability, providing a solid basis for more challenging goals in the future.

## **Objective 2**

Reaching the goal of creating, implementing and testing a control system, for monitoring marked a milestone in the project. This was achieved by utilising Proportional Derivative (PD) in Section:2.4.4 and Proportional Integral Derivative (PID) control algorithms in Section:2.5.3, which were thoroughly detailed and assessed throughout sections of the paper.

The theoretical foundation for both control methods was first confirmed through simulations that showcased their effectiveness in handling the loitering actions of the quadcopter. These simulations played a role in adjusting the control parameters and ensuring that the algorithms could function optimally in real world scenarios. Particularly the PD controller demonstrated performance during these trials showcasing a built design that effectively combined responsiveness with stability. The simulations can be viewed in sections:2.4.6 and 2.5.5.

Following this practical field tests were carried out to validate the application of the PD controller seen in Section:5.4. The outcomes were highly promising as the PD controller enabled stable loitering in changing environmental conditions. This success did not just affirm the practicality of using the PD control strategy but also underscored the improvements that incorporating the designed PID algorithm for position control would have. By employing this approach it guarantees that the quadcopter can uphold a position with minimal deviation meeting crucial needs for activities, like aerial photography, surveillance and environmental monitoring.

## **Objective 3**

The projects third objective was to perform certain hardware tasks such as proper mounting and connection of the GPS module to the on-board Raspberry Pi.

Through this project there were various different hardware tasks that needed to be completed for implementing loitering control. This included designing PCB's for various components seen in Section:3.13, as well as the soldering of the various hardware components seen in Section:3 especially the ToF sensor, GNSS modules, Barometer, Radio telemetry units and voltage regulator.

Each one of the specific hardware components I worked on played a specific role in the quadcopter, the ToF sensor was used to measure the distance, the GNSS modules were necessary for accurate positioning, the barometer provided altitude data, radio telemetry units facilitated wireless communication between the GNSS base station module and the rover module, and the voltage regulator ensured stable power supply to various components. In order for the quadcopter to function correctly these components were crucial to achieving a robust loitering control solution.

Furthermore my contribution to 3D printed components on the quadcopter should not go unnoticed. 3D printed components such as the quadcopters propeller guards, footing, motor and electronic housing played pivotal roles in both the overall quadcopters infrastructure and the protection of various different components.

Finally, due to various different crashes when testing the quadcopter in Section:??tests), I fully rebuilt the quadcopter multiple times replacing broken components for new ones, this in turn made me competent in knowing the quadcopters overall structure and how it is built which was useful when writing documentation.

## **Objective 4**

The tests I have conducted on the quadcopter were described in Section:5, they covered a wide range of topics from loitering control tests to the GNSS module's precision. All of the final tests went well, although

tuning of Proportional-Derivative (PD) controllers proved a lengthy process in order to get these results.

Moreover, I designed extensive simulations to establish a baseline for the tests that would follow. These simulations mimicked various real-world events, allowing us to modify system parameters and anticipate obstacles before actual flight tests, thus dramatically boosting the reliability and performance of the quadcopter in its loitering control capabilities.

### **Learning outcome analysis**

The project successfully achieved all the set learning goals showing an understanding and application of both knowledge and practical skills needed for creating a quadcopter that utilises loitering control.

To start I thoroughly researched various different control algorithms including Linear Quadratic Regulator (LQR), PID control, PD control and Kalman filtering, which are essential, for achieving control and state estimation in the quadcopter. The research I performed played a vital role in implementing control algorithms used in the quadcopter, improving the quadcopter's stability and precision. Moreover understanding how a GPS module works and integrating it with systems enabled real time location tracking and enhanced navigational capabilities.

When it comes to hardware design the ability to create a printed circuit board (PCB) was crucial. This skill helped in combining components into a coherent unit simplifying the design process and reducing potential issues with electronic connections. Additionally having a grasp of attitude and translational dynamics was vital for effectively handling and predicting its behavior during various flight situations.

Performing Simulations written in python prior to the tests proved very beneficial. By doing this I minimized the risks of the tests failing leading to the quadcopter crashing, optimising overall system performance. In addition I successfully mastered flying the quadcopter using the radio controller, which was crucial for manually controlling and testing automated functions.

The seamless integration of systems hardware and software components was completed. Leveraging GitHub further boosted the project's achievements by creating issues, facilitating team discussion, code reviews and helping the team work on various different parts of the project on different branches to aid development.

In essence accomplishing these learning objectives not only highlights the acquired expertise but also emphasizes the project's triumph, in developing a dependable and effective loitering control on a quadcopter.

## **6.3 Sustainability**

Throughout this project sustainable development has been constantly considered. The United States Environmental Protection Agency defines sustainable manufacturing as 'The creation of manufactured products through economically-sound processes that minimize negative environmental impacts while conserving energy and natural resources.'[19]

This project was built around sustainable practices by 3D printing components where it was viable. In contrast to traditional manufacturing techniques like machining or casting, which frequently waste material by removing it, 3D printing creates objects layer by layer, using material only where it is needed. Furthermore, there is an overall reduction in energy consumption because of the elimination of the need for producing and transporting large amounts of raw materials and the reduction in waste material that needs recycling or disposal. Finally any wasted material in the process can be recycled in order to make more parts.

In addition parts were carefully analysed for durability prior to purchase, due to the fact that more durable components will not have to be replaced as often. This will again lead to less *CO<sub>2</sub>* emissions when having to ship replacement parts. This aligns with the United Nations 9.4th target for sustainable development[20].

# Chapter 7

## Conclusions

In conclusion the GNSS base station worked very well in sending RTK corrections to the rover module figures:5.3 and 5.1 show a distinct improvement when using these corrections, Making the GNSS data accurate to  $\pm 9$ centimeters form  $\pm 1$ meter

The design of a Kalman filter to estimate position on all axis using the information from various different sensors. This objective was satisfied by a robust kalman filter design seen in Section:2.4.3. using Sensor fusion the kalman filter was developed to incorporate information from the GNSS module and ToF sensor. The kalman filter successfully filtered out noise as seen in Figure: as well as estimating accurate velocitys.

The altitude hold controller worked well when flying both indoors and outdoors with  $\pm 10$ centimetres of accuracy indoors and  $\pm 30$  outdoors. This is due to the fact that when flying outdoors the ToF sensor was subjected to uneven ground, bad weather conditions and it was also moving around.

Designing extensive simulations was paramount in successfully completing the project. They provided crucial estimates to the tuning parameters which were needed for implementation on the quadcopter for testing.

Due to various different factors position control was not tested the quadcopter as lots of time was wasted waiting for correct weather conditions as well as having to rebuild the quadcopter multiple times from crashing. Although extensive simulations were carried out as well as code implementation. This feature should be ready to test soon under the correct testing circumstances.

# Bibliography

- [1] X. Li and L. Yang, “Design and implementation of uav intelligent aerial photography system,” pp. 200–203, 2012.
- [2] F. Ondieki, O. Odongo, and L. G., “An autonomous unmanned aerial security surveillance system to enhance security in remote territories,” *International Journal of Computer Applications*, vol. 179, pp. 9–16, 12 2017.
- [3] K.-C. Weng, S.-T. Lin, C.-C. Hu, R.-T. Soong, and M.-T. Chi, “Multi-view approach for drone light show,” Nov. 2022.
- [4] K. M. Hasan, M. T. Hasan, S. S. Newaz, Abdullah-Al-Nahid, and M. S. Ahsan, “Design and development of an autonomous pesticides spraying agricultural drone,” in *2020 IEEE Region 10 Symposium (TENSYMP)*, 2020, pp. 811–814.
- [5] H.-W. Choi, H.-J. Kim, S.-K. Kim, and W. S. Na, “An overview of drone applications in the construction industry,” *Drones*, vol. 7, no. 8, 2023.
- [6] S. M. S. M. Daud, M. Y. P. M. Yusof, C. C. Heo, L. S. Khoo, M. K. C. Singh, M. S. Mahmood, and H. Nawawi, “Applications of drone in disaster management: A scoping review,” *Science & Justice*, vol. 62, no. 1, pp. 30–42, 2022.
- [7] R. K. Rangel and A. C. Terra, “Development of a surveillance tool using uav’s,” in *2018 IEEE Aerospace Conference*, 2018, pp. 1–11.
- [8] B. Mishra, D. Garg, P. Narang, and V. Mishra, “Drone-surveillance for search and rescue in natural disaster,” *Computer Communications*, vol. 156, pp. 1–10, Apr. 2020.
- [9] T. Widhianto and A. Yudhana, “System control holding position on quadcopter using gps with waypoint,” *Control Systems and Optimization Letters*, vol. 1, pp. 12–18, 03 2023.
- [10] P. A. Baru, S. Sabikan, and S. Nawawi, “Open-source project (osps) platform for outdoor quadcopter,” *Journal of Advanced Research Design*, vol. 24, no. 1, 2016.
- [11] A. H. Ahmed, A. N. Ouda, A. M. Kamel, and Y. Z. Elhalwagy, “Attitude stabilization and altitude control of quadrotor,” pp. 123–130, 2016.
- [12] P. Karthik, K. Kumar, V. Fernandes, and K. Arya, “Reinforcement learning for altitude hold and path planning in a quadcopter,” pp. 463–467, 2020.

- [13] J. B. Kuipers, *Quaternions and Rotation Sequences: A Primer with Applications to Orbits, Aerospace, and Virtual Reality*. Princeton University Press, 1999, accessed: Mar. 27, 2024. [Online]. Available: [https://books.google.co.uk/books?hl=en&lr=&id=\\_Og9DwAAQBAJ&oi=fnd&pg=PR21&dq=Kuipers](https://books.google.co.uk/books?hl=en&lr=&id=_Og9DwAAQBAJ&oi=fnd&pg=PR21&dq=Kuipers)
- [14] K. Shoemake, “Animating rotation with quaternion curves,” *SIGGRAPH Comput. Graph.*, vol. 19, no. 3, p. 245–254, 1985.
- [15] E. Fresk and G. Nikolakopoulos, “Full quaternion based attitude control for a quadrotor,” IEEE, pp. 3864–3869, 2013.
- [16] E. Small, P. Sopasakis, E. Fresk, P. Patrinos, and G. Nikolakopoulos, “Aerial navigation in obstructed environments with embedded nonlinear model predictive control,” Accessed: Apr. 23, 2024, Apr. 2024.
- [17] SBG Systems, “Real time operation with cm level accuracy,” 2024, accessed: 2024-03-27, Page: 91. [Online]. Available: <https://support.sbg-systems.com/sc/kb/latest/inertial-sensors-operation/real-time-operation-with-cm-level-accuracy>
- [18] A. Bashyam and J. Guggenheim, “Uavs for wilderness search and rescue: Real-world considerations and technology roadmap for fixed wing uavs,” 2019.
- [19] Environmental Protection Agency, “Sustainable manufacturing,” 2023, accessed: 2023-04-21. [Online]. Available: <https://www.epa.gov/sustainability/sustainable-manufacturing>
- [20] United Nations, “Goal 9: Build resilient infrastructure, promote inclusive and sustainable industrialization and foster innovation,” Sustainable Development Goals, 2023, accessed: 2023-04-21. [Online]. Available: [https://sdgs.un.org/goals/goal9#progress\\_and\\_info](https://sdgs.un.org/goals/goal9#progress_and_info)